Chlordecone-induced hepatotoxicity and fibrosis are mediated by the proteasomal degradation of septins

Thibaut Léger, Sarah Alilat, Pierre-Jean Ferron, Léonie Dec, Tahar Bouceba, Rachelle Lanceleur, Sylvie Huet, Yoann Devriendt-Renault, Julien Parinet, Bruno Clément, et al.

▶ **To cite this version:**

Thibaut Léger, Sarah Alilat, Pierre-Jean Ferron, Léonie Dec, Tahar Bouceba, et al.. Chlordecone-induced hepatotoxicity and fibrosis are mediated by the proteasomal degradation of septins. Journal of Hazardous Materials, 2024, 476, pp.135177. 10.1016/j.jhazmat.2024.135177 . anses-04661415

HAL Id: anses-04661415

https://anses.hal.science/anses-04661415

Submitted on 24 Jul 2024

HAL is a multi-disciplinary open access archive for the deposit and dissemination of scientific research documents, whether they are published or not. The documents may come from teaching and research institutions in France or abroad, or from public or private research centers.

L'archive ouverte pluridisciplinaire **HAL**, est destinée au dépôt et à la diffusion de documents scientifiques de niveau recherche, publiés ou non, émanant des établissements d'enseignement et de recherche français ou étrangers, des laboratoires publics ou privés.

Distributed under a Creative Commons Attribution 4.0 International License

Journal of Hazardous Materials 476 (2024) 135177

Contents lists available at ScienceDirect

Journal of Hazardous Materials

journal homepage: www.elsevier.com/locate/jhazmat

Chlordecone-induced hepatotoxicity and fibrosis are mediated by the proteasomal degradation of septins

Thibaut Léger [a,*], Sarah Alilat [a], Pierre-Jean Ferron [b], Léonie Dec [a], Tahar Bouceba [c], Rachelle Lanceleur [a], Sylvie Huet [a], Yoann Devriendt-Renault [d], Julien Parinet [d], Bruno Clément [b], Valérie Fessard [a], Ludovic Le Hégarat [a]

[a] ANSES, French Agency for Food, Environmental and Occupational Health & Safety, Toxicology of Contaminants Unit, Fougères Laboratory, 35306 Fougères CEDEX, France
[b] INSERM, University of Rennes, INRAE, Institut NuMeCan (Nutrition, Metabolisms and Cancer) UMR_A 1317, UMR_S 1241, Previtox Network, 35000 Rennes, France
[c] Sorbonne University, CNRS, Institut de Biologie Paris-Seine (IBPS), Protein Engineering Platform, Molecular Interaction Service, Paris, France
[d] ANSES, French Agency for Food, Environmental and Occupational Health & Safety, Pesticides and Marine Biotoxins (PBM) unit, Maison-Alfort Laboratory, 94701 Maison-Alfort CEDEX, France

HIGHLIGHTS

- Hepatocytes are more sensitive to CLD than CLDOH, its major metabolite.
- CLD is sequestered whereas CLDOH is rapidly glucuronide-conjugated and excreted.
- CLD but not CLDOH hepatotoxicity is driven by proteasomal degradation of septins.
- CLD disrupts LD and BA secretion and increases DCA production.
- Fibrosis is triggered by CLD in the absence of a fat overload in liver organoids.

GRAPHICAL ABSTRACT

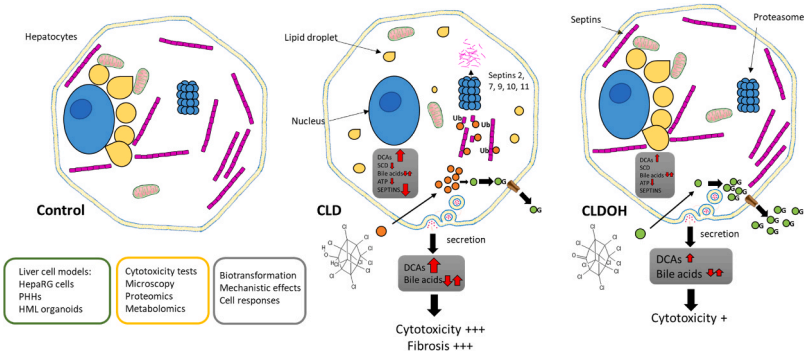

ARTICLE INFO

Keywords:
Pesticide
MASLD
Hepatocytes
Organoids
Multiomics

ABSTRACT

Chlordecone (CLD) is a pesticide persisting in soils and contaminating food webs. CLD is sequestered in the liver and poorly metabolized into chlordecol (CLDOH). In vitro liver cell models were used to investigate the fate and mechanistic effects of CLD and CLDOH using multiomics. A 3D-cell model was used to investigate whether CLD and CLDOH can affect susceptibility to the metabolic dysfunction-associated steatotic liver disease (MASLD). Hepatocytes were more sensitive to CLD than CLDOH. CLDOH was intensively metabolized into a glucuronide conjugate, whereas CLD was sequestered. CLD but not CLDOH induced a depletion of Septin-2,– 7,– 9,– 10,– 11 due to proteasomal degradation. Septin binding with CLD and CLDOH was confirmed by surface plasmon

Abbreviations: BA, bile acid; CLD, chlordecone; CLDOH, chlordecol; DCA, dicarboxylic acid; FAO, fatty acid oxidation; FWI, French West Indies; HCC, hepatocellular carcinoma; HCS, high-content screening; HML, HepaRG/Macrophages/LX-2; LD, lipid droplet; MS/MS, tandem mass spectrometry; MASLD, non-alcoholic fatty liver disease; NASH, non-alcoholic steatohepatitis; OXPHOS, oxidative phosphorylation; PHH, primary human hepatocyte; ROS, reactive oxygen species; SCD, stearoyl-CoA desaturase; SPR, surface plasmon resonance.

* Corresponding author.
E-mail address: thibaut.leger@anses.fr (T. Léger).

https://doi.org/10.1016/j.jhazmat.2024.135177
Received 29 March 2024; Received in revised form 8 July 2024; Accepted 9 July 2024
Available online 11 July 2024
0304-3894/© 2024 The Author(s). Published by Elsevier B.V. This is an open access article under the CC BY license (http://creativecommons.org/licenses/by/4.0/).

resonance. CLD disrupted lipid droplet size and increased saturated long-chain dicarboxylic acid production by inhibiting stearoyl-CoA desaturase (SCD) abundance. Neither CLD nor CLDOH induced steatosis, but CLD induced fibrosis in the 3D model of MASLD. To conclude, CLD hepatoxicity is specifically driven by the degradation of septins. CLDOH, was too rapidly metabolized to induce septin degradation. We show that the conversion of CLD to CLDOH reduced hepatotoxicity and fibrosis in liver organoids. This suggests that protective strategies could be explored to reduce the hepatotoxicity of CLD.

1. Introduction

Metabolic dysfunction-associated steatotic liver disease (MASLD), which includes liver steatosis and steatohepatitis with or without fibrosis, is a major risk factor for the development of hepatocellular carcinoma (HCC). The prevalence of MASLD worldwide was reported as around 32 % [1]. MASLD susceptibility is multifactorial, being linked to genetics, epigenetics, diet, and a sedentary lifestyle among others, but also exposure to environmental contaminants [2]. MASLD has been shown to be affected by exposure to some pesticides [3] such as vinyl chlorine [4], benzene [5], perfluoroalkyl substances (PFASs) [3] and other persistent organic pollutants (POPs) [6]. However, the mechanisms of action of chemicals leading to MASLD remain largely unknown [3,7], particularly those of organochlorine pesticides [8-10].

Chlordecone (CLD) is an organochlorine pesticide used to control the banana weevil *Cosmopolites sordidus* in the French West Indies (FWI) from 1970 to 1993. Despite its ban by France in the 90 s, its high persistence in soil [11] has enhanced the transfer into agricultural food resources as well as into other environmental compartments and the organisms living in these ecosystems [12], raising major concerns for environmental and public health [13]. Besides neurological symptoms (i.e., tremors, ataxia), chlordecone-exposed workers in the Hopewell plant in Virginia, USA, showed hepatic concentrations ranging from 27 to 350 μM with a liver to blood concentration ratio of 15 [14], revealing that the liver is a preferred target of CLD exposure. Moreover, Hopewell workers developed mild steatosis, portal inflammation and fibrosis [15]. A recent report estimated that 92 % of Guadeloupeans and 95 % of Martinicans were exposed in 2014 above the limit of quantification for chlordecone (0.041 nM or 0.02 μg/L in plasma), with 14 % and 25 %, respectively, exceeding the chronic internal toxicity reference value, established at 0.81 nM (0.4 μg/L in plasma) ([16]; DREES-Insee [17]; EPA [18]; Santé publique France [19]).

Epidemiological studies have suggested that CLD could be involved in prostate cancer [20,21], might also impair neurodevelopment and cognitive abilities [22,20,23]. CLD has also been described as an endocrine disruptor [24-27]. In the liver, CLD has been shown to induce hepatic dysfunctions [28] and hepatocellular hypertrophy, to increase liver size in humans [15] and rats [29], to potentiate fibrosis induced by drugs such as carbon tetrachloride [30] and to promote liver tumors in rats and mice [31,32]. Nevertheless, the prevalence of liver cancer in the FWI was reported to be lower than in metropolitan France (Santé publique France, 2019). In humans and animals, CLD is metabolized into chlordecol (CLDOH), the major phase I metabolite [33]. The CLD ketone group is reduced to alcohol by the liver-specific aldoketoreductase AKR1C4 to form CLDOH. Although this metabolic pathway has mainly been observed in humans, pigs, gerbils, and rabbits, less CLDOH was formed in rats and mice [34]. Glucuronidated and sulfated forms have been described as major phase II metabolites of CLD. They are excreted mainly by the fecal route as deconjugated forms [33]. A high level of CLDOH (ratio 3:1 compared with CLD) has been reported in human bile after a glucuronide deconjugation step. In rats, CLD diffuses into different tissues, but mainly the liver, where it is sequestered [35]. However, it also reaches fat and brain tissue, though in smaller quantities (EPA, 2009). Despite detoxification, CLD has been shown to be sequestered in the human body, particularly in the liver according to human physiologically-based pharmacokinetic models based on rats [35,36]. Both enterohepatic cycle reabsorption and sequestration by chlordecone-binding proteins (CDBPs) in liver cells [36] can explain CLD persistence in the human body, a long half-life in workers (max. 148 days) having been reported [14]. Moreover, CLD and CLDOH display affinity for plasma proteins such as lipoproteins [37], and CLD has also been reported to bind albumin [38].

Although some cellular effects of CLD on liver—such as adenosine triphosphate hydrolase (ATPase) inhibition and induction of cytochrome P450—have been reported [39], the mechanisms involved in CLD hepatotoxicity remain unclear.

The present study analyzed the molecular mechanisms involved in CLD hepatotoxicity as well as the impact of metabolization through liver hepatic cell models (both HepaRG cells and primary human hepatocytes) exposed to CLD and CLDOH, using metabolomics and proteomics. Both kinetic and dose-response studies were carried out. Furthermore, given the 25 % prevalence of obesity in the FWI (10 % higher than in metropolitan France) observed in 2019 (DREES-Insee, 2021) and its relationship with liver pathologies [28], the effects of CLD and CLDOH on the progression of MASLD were also assessed using an organoid model mimicking MASLD.

2. Experimental Procedures

2.1. Reagents

Chlordecone (≥ 98 %) and chlordecol (≥ 98 %) were purchased from Azur Isotopes SAS (Marseille, France). Ronidazole-d3, MG132 (≥ 90 %), bafilomycin A1 (≥ 90 %), and tamoxifen (≥ 98 %) were purchased from Sigma-Aldrich (St. Louis, MO, USA). Erythromycin-d6 was purchased from Toronto Research Chemicals (North York, ON, Canada). Flunixin-d3 and albendazole-d3 were purchased from Witega Laboratorien Berlin-Adlershof GmbH (Berlin, Germany). Forchlorfenuron (≥ 90 %), liquid chromatography–mass spectrometry (LC-MS) grade acetonitrile, methanol, and water were purchased from Fisher Scientific (Waltham, MA, USA).

2.2. Cell culture

The culture of the human hepatic cell line HepaRG (Biopredic International, Rennes, France) has already been described [40]. This protocol leads to a mixture of both cholangiocyte- and hepatocyte-like cell populations after a 15-day differentiation period [41]. Cryopreserved PHHs derived from a 67-year old Caucasian male (Batch number: HEP187436-PA05) suffering from liver metastases from colorectal cancer (cause of death) were obtained from Biopredic International (Saint-Grégoire, France). The PHHs were cultured as previously described [40] and according to the supplier's protocol. For HepaRG/Macrophages/LX-2 (HML) organoids, HepaRG cells were cultured following the previously described method, except that differentiation was obtained using 2 % DMSO. Human macrophages were differentiated from peripheral blood mononuclear cells as previously described [42]. Peripheral blood mononuclear cells were isolated from buffy coat donations obtained from the French Blood Agency (Etablissement Français du Sang, Rennes, France). Monocytes were enriched using a human CD14 separation kit (Microbeads; MiltenyiBiotec, Bergisch Gladbach, Germany). Macrophages were obtained from monocytes after differentiation. LX2 cells, provided by S.L. Friedman (Icahn School of Medicine at Mount Sinai, New York, USA), were cultivated in

an activated state, as previously described [43]. Detailed protocols are presented in the Supplementary Materials and Methods section.

2.3. Production of HepaRG/Macrophages/LX-2 Organoids and steatosis and fibrosis induction

HML organoids were generated by seeding a solution of isolated cells in a Sigma micro-mold system (Z764051–6EA; Sigma, St. Louis, MO, USA), following the method described previously [44]. Cells were seeded at a density of 2000 cells per organoid, with a ratio of 80 % differentiated HepaRG, 10 % macrophages, and 10 % LX-2 cells. After 3 days of culture, the FBS concentration was reduced to 1 %. Treatments with CLD and CLDOH began at 8 days of culture. Medium with CLD and CLDOH was renew at 11 and 13 days of culture, prior to organoid harvest after 14 days of culture.

For steatosis and fibrosis induction, HML organoids were treated with a mixture of fatty acids to induce steatosis as previously described [44]. The mixture is composed of 150 μM stearic acid and 300 μM oleic acid (both from Sigma-Aldrich) prepared in fatty acid-free BSA. Treatments started on day 5 after seeding and were repeated every other day until day 14 of culture. Detailed procedures are presented in the Supplementary Materials and Methods section.

2.4. Cell treatments

2D HepaRG cells were used in 12-well plates for (i) a concentration-response experiment after 24-hour exposure to 1 and 5 μM CLD and 1, 5, and 10 μM CLDOH and (ii) a kinetic experiment with 3-, 8-, 24- and 48-hour time points at 5 μM CLD and at 5 and 10 μM CLDOH. Solvent controls (0.1 % DMSO) were used for each time point. Triplicate wells were used for each treatment condition. For PHHs, CLD and CLDOH were incubated for 24 h at 5 and 10 μM, respectively, in medium supplemented with 0.1 % DMSO. For the controls, the cell medium was supplemented with 0.1 % DMSO. After treatment, cell culture media were collected and frozen at − 80 °C. Cells were washed and lysed before omics analyses as previously described [40]. Both cell culture media and cell lysates were analyzed by metabolomics, whereas only cell lysates were investigated by proteomics. To test proteasomal and lysosomal degradation, HepaRG cells were incubated for 24 h with, respectively, 10 μM MG132 and 10 nM bafilomycin A1 (Baf) in combination with, or without, 5 μM CLD or 10 μM CLDOH. For organoids, CLD and CLDOH were dissolved in DMSO and diluted in cell culture medium. After treatment, HML organoids were harvested and fixed in 5 % formalin during 1 h and washed in PBS. Organoids were embedded in paraffin and 4 μm sections were cut at 4 μm. HML organoids were generated in a 96-well round bottom ultra-low attachment plate to evaluate drug toxicity. On day 8, 80 % of the well medium was renewed with medium containing compounds prepared in 0.5 % DMSO. The medium was renewed on D11 and D13 prior to further analysis. Detailed procedures are presented in the Supplementary Materials and Methods section.

2.5. Cell viability testing

Prior to multiomic experiments, we determined the maximum concentrations of CLD and CLDOH that did not alter cell viability. Twenty-four hours after seeding on 12-well and 24-well plates, hepatocytes (HepaRG, PHHs) were exposed to increasing concentrations of CLD and CLDOH for 24 h. After 24-hour exposure, cytotoxicity was evaluated with an MTT (3- [4,5- dimethylthiazol-2-yl]−2,5-diphenyl tetrazolium bromide) assay kit from Sigma Aldrich (St. Louis, MO, USA) with the concentrations of CLD and CLDOH ranging from 0.31 to 20 μM for HepaRG cells, and from 1.25 to 40 μM for PHHs. The viability of HML organoids was measured after 7 days of treatment with CLD and CLDOH using the CellTiter-Glo® Luminescent Cell Viability assay (Promega, Charbonnières, France) following the manufacturer's instructions. The luminescent signal was quantified using a POLARstar® Omega microplate reader (BMG Labtech, Ortenberg, Germany). Detailed procedures are presented in the Supplementary Materials and Methods section.

2.6. Measurement of ATP and ROS levels

The cellular adenosine triphosphate (ATP) level was determined for 2D HepaRG cells and PHHs using the CellTiter-Glo® Luminescent Cell Viability assay according to our previous work [40]. Reactive oxygen species (ROS) generation was measured in 2D HepaRG cells using 2′, 7′-dichlorodihydrofluorescein diacetate (DCFDA) and Hoechst 33342 nuclear dye as previously described [40]. Tebufenpyrad, an inhibitor of the mitochondrial complex I, was used as a positive control (at 10 μM).

2.7. Staining and immunolabeling of 2D HepaRG cells and HML organoids

2D HepaRG cells were labeled with primary antibodies targeting Septin-9 (sc-293291, Santa Cruz Biotech), Septin-2 (NBP1–06076, Novus Biologicals), and Lamp-1 (ab24170, Abcam). Phalloidin-FITC (P5282, Sigma Aldrich) and DAPI (D9542, Sigma Aldrich) were used. BODIPY 493/503 (#790389, Sigma Aldrich) was used to visualize neutral lipids and triglycerides in lipid droplets. 2D HepaRG cells were immunolabeled in biological triplicates. Imaging was acquired with an ArrayScan VTI HCS Reader (Thermo Scientific, Waltham, USA) system at 20X magnification and analyses with the HCS studio software (Thermo Scientific, Waltham, USA).

For staining and immunolabeling of HML organoids, each paraffin section was stained by hematoxylin and eosin (H&E) and the best ones were selected for immunochemical labeling using rabbit anti-Col1A1 (ab34710, Abcam), mouse anti-Col4 (CIV22) (DAKO _M0785) and mouse anti-Vimentin (V9-(3)) (DAKO_ M0725). The labeling was performed on a Discovery ULTRA automated IHC stainer (ROCHE) using the Ventana detection kit (Ventana Medical Systems, Tucson, Arizona). To visualize nuclei, DAPI staining was added. Slides were scanned on a Pannoramic confocal scanner (3DHISTECH Ltd., Budapest, Hungary) at 20X magnification.

2.8. Steatosis and fibrosis quantification

Steatosis release and progression were evaluated by quantifying neutral lipids and triglycerides using BODIPY 493/503. The stained HML organoids were acquired using a CellCyte X (Cytena, Freiburg, Germany), and image analysis was performed using Cellcyte Studio (Cytena, Germany). For fibrosis quantification, the images for nuclei (DAPI), collagen 1 (COL1) and collagen 4 (COL4) quantifications were acquired and stored in TIFF format. Images were analyzed using ImageJ FIJI software v1.53 and Trackmate CellPose plugin v0.1.2. The TIFF images were preprocessed before analysis to crop organoids and to separate the blue and red channels corresponding to nuclei and COL1/4, respectively. Nuclei of each organoid were counted using CellPose and segment nuclei function. Three organoids were used for each experimental condition. Then, to estimate fibrosis, the total intensity for the red channel was quantified for each organoid and reported relative to the number of nuclei per organoid.

2.9. Metabolomic data acquisition

Metabolites present in the cell culture media (500 μL) and cell lysates (100 μg) were extracted and concentrated using a Strata-X 96-well plate (30 mg, Phenomenex). For each experimental triplicate, metabolites were analyzed by a Q-Exactive mass spectrometer coupled to a Vanquish Flex Binary UHPLC system (both from Thermo Scientific) in negative ionization mode. Three to five quality control (QC) samples were included to check acquisition reproducibility. Parameters used for chromatographic separations and MS acquisitions have been described

previously [40]. Detailed protocols are presented in the Supplementary Materials and Methods section.

2.10. Quantification and statistical analyses of metabolomic data

Except for the maximum element parameter set to $C_{90}H1_{90}Cl_{20}K_2N_{10}Na_2O_{18}P_3S_5$, which indicates the maximum number of each element for the annotations of CLD and CLDOH and their metabolites, the retention alignment step and the detection parameters for Compound Discoverer 3.2 software (Thermo Scientific) were used as previously described [40]. Moreover, data normalization and a QC correction were applied to each dataset (Supplementary Fig. S1). Both a database for endogenous metabolites (4400 entries, Thermo Scientific) and an in-house database of metabolites specific to HepaRG cells were used. Metabolites were annotated using Chemspider and the predicted compositions algorithm of Compound Discoverer. Metabolite identification was validated with Mzcloud using MS2 spectra and with linear correlations of RT with XLogP3 and LogP of metabolites. A linear correlation with an R^2 of 0.745 was obtained (Supplementary Fig. S2). Neutral losses (61 species) were scanned in MS2 spectra to detect potential phase I and II metabolites as previously described. P-values per group ratio were calculated by a one-way ANOVA model with Tukey as a post-hoc test and adjusted with a Benjamini-Hochberg correction. A threshold of 0.05 was used to consider further abundance variations of metabolites. The selection criteria for metabolites of interest were: (i) their annotation based on the Schymanski classification [45], (ii) their significance in terms of variation in abundance (p-value threshold <0.05), (iii) their belonging to families of compounds such as bile acids (BAs) or dicarboxylic acids (DCAs).

2.11. Proteomic data acquisition

Each sample's protein concentration was determined using a BiCinchoninic acid (BCA) protein assay (Thermo Scientific). Protein extracts from triplicate cell lysates (100 µg) were precipitated, reduced, alkylated and digested by trypsin as described in our previous study [40]. Peptides were desalted and analyzed by a Q-Exactive mass spectrometer coupled to a Vanquish Flex Binary UHPLC system (both from Thermo Scientific). Chromatographic separation conditions were those described in our previous work [40]. Detailed protocols are presented in the Supplementary Materials and Methods section.

2.12. Quantification and statistical analyses of proteomic data

All MS/MS data and statistical analyses were processed with the parameter settings of, respectively, Maxquant (version 2.0.3.1) and Perseus software (version 1.6.15) as described previously [40]. Variations in protein abundance were only considered for calculated ANOVA p-values below 0.05. A Student t-test was applied with a permutation-based FDR threshold at 0.05 for each binary comparison. An unsupervised Bayesian clustering [46] with proteins having an ANOVA p-value below 0.05 was performed using normalized abundance values by mean. Analyses of gene ontology (GO) term enrichment were carried out for each generated cluster using the Cluego Cytoscape plug-in [47]. For proteasomal degradation testing using MG132, two-way ANOVA p-values were calculated to test the interaction between CLD or CLDOH and MG132. Detailed protocols are presented in the Supplementary Materials and Methods section.

2.13. Absolute quantification of CLD and CLDOH

To prepare each sample, 0.05 g of culture medium was collected and placed into a 50 mL centrifuge tube prior to the addition of 10 µL of CLD and CLDOH isotopic standard mix (13C8-CLD and 13C8-CLDOH) at 25 µg/mL. A QuEChERS extraction kit was used. The HPLC-MS/MS parameters have been described previously [48]. Briefly, an Aqua C18 precolumn (4.0 mm × 2.0 mm×3 µm) and an Aqua C18 column (150 mm × 2.0 mm×3.0 µm) supplied by Phenomenex (Torrance, CA) were used for chromatographic separation on an Agilent 1200 series binary pump and autosampler coupled to a 5500 Q-Trap AB SciEX mass spectrometer (Darmstadt, Germany). Two single reaction monitoring (SRM) were set for both CLD (506.7/426.7 and 508.7/428.7) and CLDOH (490.7/35.0 and 492.7/35.0). The limit of detection (LOD) was established at one third of the lowest verified residue level, which was set as the LOQ. For CLD and CLDOH, the LOD and LOQ were set to 7 and 20 ng. g^{-1}, respectively. To measure the CLD and CLDOH concentrations in the culture medium, the same chemicals, reagents, equipment, and apparatus were used as described previously [48]. Detailed protocols are presented in the Supplementary Materials and Methods section.

2.14. Molecular docking

3D structure data files for SEPT2 (2QNR), SEPT3 (3SOP) [49], and SEPT7 (3T5D) [50] in a complex with GDP and Mg^{2+} were obtained from the RCSB protein databank (PDB) website (https://www.rcsb.org/). The online docking web server DockThor (Guedes et al., 2021) was used with a standard search algorithm precision and the same parameters as described previously [40]. Blind docking experiments were completed for SEPT2, SEPT3, and SEPT7 using GDP, forchlorfenuron and tebufenpyrad (TEBU). Affinity prediction values (kcal/mol) were compared when binding sites were similar. Detailed protocols are presented in the Supplementary Materials and Methods section.

2.15. Surface plasmon resonance

SPR experiments were performed on a Biacore 3000 instrument (GE Healthcare) at the Platform of Molecular Interactions, Institute of Biology Paris Seine (IBPS, Sorbonne University). All experiments were performed in duplicate, as described previously [51] at 25 °C in HBS-EP running buffer. Recombinant SEPT2 (AB99296, Abcam) was covalently immobilized through primary amino groups to the carboxy-methylated dextran matrix of a CM5 sensor chip (Cytiva). CLD and CLDOH were evaluated as ligands and TEBU, tamoxifen, and forchlorfenuron (50 µM, 20 µL/min for 3 min) were used as controls. The sensorgrams were evaluated using the BIA evaluation software, version 4.1 (Cytiva). Detailed protocols are presented in the Supplementary Materials and Methods section.

2.16. Statistical analysis

Unless stated differently, all data are represented as mean ± SD values. All p values < 0.05 were considered significant *$p < 0.05$, * *$p < 0.01$, and * **$p < 0.001$. All experiments were performed at least three times. All statistical analyses were performed on GraphPad Prism 8 using paired two-tailed Student's t-test except omics data, for which dedicated tools were used.

3. Results

3.1. Cytotoxicity of CLD and CLDOH on HepaRG cells and PHHs

HepaRG cells were less sensitive to CLDOH than CLD according to the cytotoxicity results (Fig. 1A, top panel). Cell viability decreased by 8 % and 44 % following 24-hour exposure to 10 µM CLDOH and CLD, respectively. Similar toxicity results with CLDOH and CLD were observed on PHHs (Fig. 1A, bottom panel).

3.2. CLD and CLDOH induced slight decreases in ATP levels but no variation in ROS levels

No decrease in ATP level was observed in HepaRG cells following 24 h of CLD and CLDOH treatment (Fig. 1B). At 24 h, no decrease in ATP

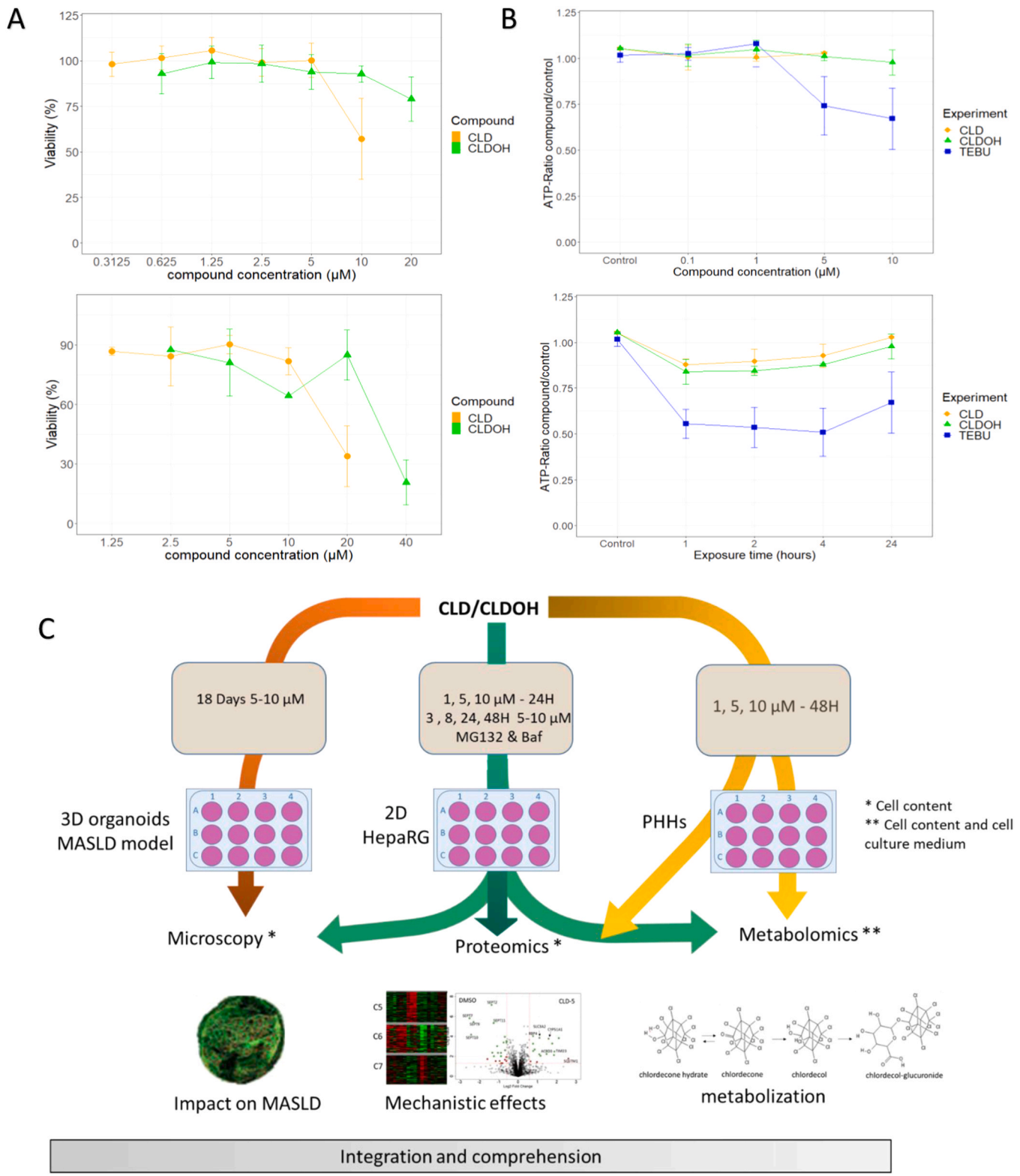

Fig. 1. Cytotoxicity of CLD and CLDOH and omics workflow. (A) CLD and CLDOH cytotoxicity by MTT assay in HepaRG cells (top panel) and PHHs (bottom panel) at 24-hour exposure. (B) ATP levels measured in HepaRG cells following CLD and CLDOH exposure. The top panel showed a concentration-response experiment at 24-hour exposure. The bottom panel shows a kinetic experiment with CLD and CLDOH concentrations of 5 and 10 μM, respectively. (C) Experimental workflow including cell types, exposure conditions, and multiomic experiments.

was noted with concentrations from 0.1 to 10 μM (Fig. 1B, top panel). However, a decrease in ATP level was observed for both CLD and CLDOH up to 1 h of exposure (Fig. 1B, bottom panel), a decrease clearly compensated for after 24 h. No variation in ROS level was induced in HepaRG cells after acute CLD and CLDOH exposure up to 24 h (Supplementary Fig. S3). Concentrations of CLD and CLDOH that do not alter the viability of HepaRG cells and PHHs, i.e., 5 μM CLD and 10 μM CLDOH, were chosen to investigate their mechanism of action in liver

cells by omic analyses. Their effects were investigated in concentration-response and kinetic experiments in HepaRG cells and PHHs (Fig. 1C). Proteomic and metabolomic analyses were conducted on intracellular contents. Additional metabolomic analyses were carried out on cell culture medium to study the fate of CLD and CLDOH, including the formation of metabolites.

3.3. Metabolization of CLD and CLDOH in HepaRG cells

Absolute quantification by LC MS/MS of CLD and CLDOH in cell culture medium at 1 µM and 5 µM exposure up to 24 h showed that CLD disappeared more rapidly than CLDOH. Indeed, 82.8 % and 50.8 % of CLD and CLDOH (1 µM), respectively, disappeared after 1 h of exposure (Supplementary Table S1). However, CLDOH disappeared completely with a concentration below the LOD at 8 h whereas the CLD concentration remained at 12 % at 24 h of exposure (1 µM).

The fate of CLD, CLDOH, and CLDOH-glucuronide (CLDOH-G) was also examined by metabolomics through concentration-response and kinetic studies in cell culture medium and cell content (Fig. 2A, Supplementary File S1). It should be noted that, unlike absolute

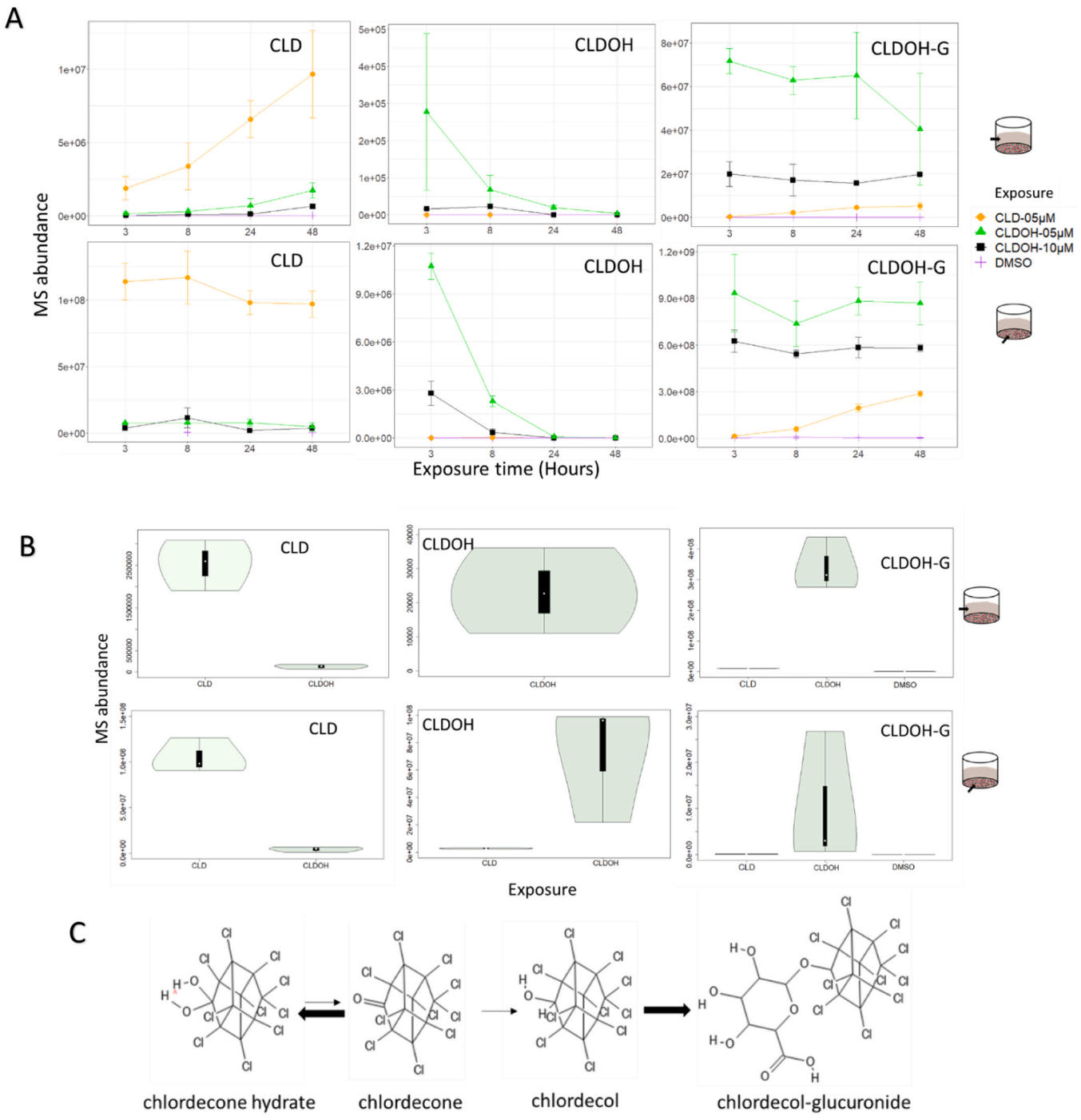

Fig. 2. CLD and CLDOH metabolisation by HepaRG cells and PHHs. (A) Unscaled trendline charts showing variations in CLD and CLDOH metabolite abundance in HepaRG cells according to exposure time (3, 8, 24, 48 h), obtained by metabolomics. Extra- (top panel) and intracellular abundance of CLD, CLDOH, and CLDOH glucuronide. (B) Extra- (top panel) and intracellular abundance of CLD, CLDOH and the glucuronide form after treatment of PHHs with CLD and CLDOH. (C) CLD and CLDOH metabolism adapted from EPA (EPA, 2009). The full dataset is presented in Supplementary File S1.

quantification results, an increase in CLD abundance (hydrated form) at a very low abundance in the cell culture medium was observed from 3 h of exposure and throughout the treatment (48 h maximum). Secondly, CLD could also form dimers, detected by metabolomics (Supplementary File S1). CLD accumulated more in cells than CLDOH (abundance ratio between intracellular and extracellular medium of 360 and 43 at 24 h for CLD (hydrated form) and CLDOH, respectively (Fig. 2A). This was consistent with a higher rate of CLDOH metabolization into glucuronidated metabolites. No formation of CLD glucuronide was observed, whatever the conditions tested. Glucuronidated forms (CLDOH-G) of CLD and CLDOH accumulated in cell culture medium with an intracellular/extracellular ratio of 0.03 and 0.12 for, respectively, CLD and CLDOH after 48 h of exposure (Fig. 2A). CLDOH conversion to glucuronidated forms was complete between 3 and 8 h, as shown by the stable

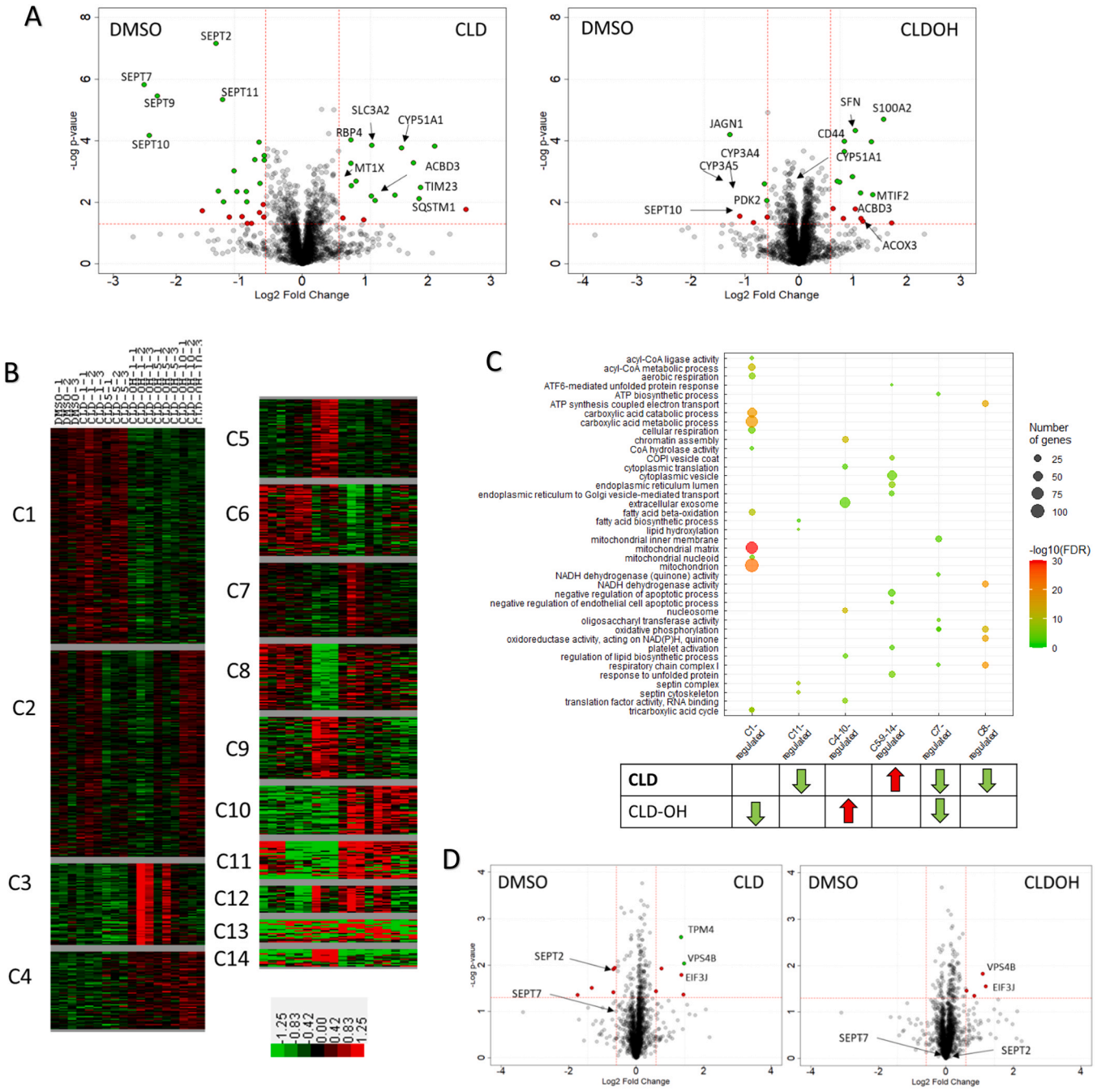

Fig. 3. Proteomic analyses of intracellular protein contents from dose-response experiments with CLD and CLDOH on HepaRG cells and PHHs. (A) Volcano plots of the proteins expressed following CLD (5 μM) and CLDOH (10 μM) treatment of HepaRG cells. P-values were calculated using two-sided Student's t-tests. Red dots represent proteins with p-values between 0.01 and 0.05, and a fold change greater than 1.5. Green dots represent proteins with p-values lower than 0.01, and a fold change greater than 1.5. The full dataset is presented in Supplementary File S2. (B) Classification of differentially expressed proteins from HepaRG cells by the unsupervised bayesian clustering AutoClassWeb application. Proteins with an Anova p-value lower than 0.05 were selected. Reported values are abundance values normalized by means. The full dataset is presented in Supplementary File S4. (C) Gene Ontology term enrichment analyses of proteins belonging to selected clusters generated in Fig. 3B. P-values were calculated using a hypergeometric test and adjusted with a Benjamini-Hochberg multiple test correction. The full dataset is presented in Supplementary File S5. (D) Volcano plots representing protein abundance values following treatment of PHHs with CLD (5 μM) and CLDOH (10 μM). The full dataset is presented in Supplementary File S2.

level of metabolites detected in the extracellular medium after 8 h. Concomitantly, the level of CLDOH-G decreased inside the cells (Fig. 2A). In contrast, following CLD exposure, the abundance of CLDOH-G increased up to 48 h of exposure in both intra- and extracellular media. These results clearly indicate that CLD was minimally converted into CLDOH-G forms and remained sequestered inside liver cells, while CLDOH was intensively converted to CLDOH-G and rapidly excreted. Nevertheless, abundance of enzyme AKR1C4, which converts CLD to CLDOH, was unaffected according to the proteomic dataset (Supplementary File S2). In PHHs, CLD—unlike CLDOH—was shown to be minimally converted into CLDOH-G, accumulating inside the cells (Fig. 2B). A scheme of CLD and CLDOH global metabolism is proposed (Fig. 2C).

3.4. CLD and CLDOH effects on hepatocyte metabolism

Proteins with differential abundance following CLD and CLDOH treatment of HepaRG cells are shown in volcano plots (Fig. 3A, Supplementary Fig. S4A) and in the non-supervised Bayesian clustering representation (Fig. 3B, Supplementary File S3). Liver cell metabolism was not affected equally by CLD and CLDOH, as revealed by gene ontology term enrichment analyses (Fig. 3C, Supplementary File S4). Both CLD and CLDOH slightly decreased the abundance of proteins implicated in OXPHOS. However, CLDOH also induced a slight decrease in proteins involved in mitochondrial respiratory complexes, mitochondrial biogenesis and FAO, while CLD decreased the abundance of cytoskeletal septins in both concentration-response (Fig. 3A, Fig. 3C) and kinetic (Supplementary Fig. S5) experiments. Lipid metabolism perturbations were also noticed with CLD treatment. For example, CYP51A1—implicated in cholesterol synthesis—specifically increased in abundance following CLD exposure in both kinetic and concentration-response experiments, whereas the abundance of stearoyl-CoA desaturase (SCD) decreased (Fig. 3A, Supplementary Fig. S6). Abundance of CYP2E1 and CYP3A4, oxidases implicated in fatty acid hydroxylation, decreased following CLD exposure in both HepaRG cells (Supplementary Fig. S5 and File S2) and PHHs (Supplementary File S2). CLD increased the abundance of proteins associated with transport via the endoplasmic reticulum, while CLDOH increased those involved in cytoplasmic translation. In PHHs, CLD and CLDOH hardly affected liver metabolism (Fig. 3D, Supplementary Fig. S4B).

3.5. CLD induces septin proteasomal degradation

The abundance of septin-2, − 7, − 8, − 9, − 10, and − 11 decreased after CLD exposure (Fig. 3A). For example, SEPT7 had decreased by more than 70 % at 48 h with 5 μM CLD. For all the septins, the decrease induced by CLD occurred as early as 8 h and lasted throughout the 48 h of treatment (Fig. 4A) and was dose-dependent (Fig. 4B). In contrast, CLDOH did not affect the abundance of septins, irrespective of time and concentration (Fig. 3A, Fig. 4A, Fig. 4B). No effect was reported on other components of the cytoskeleton such as cadherins, catenins or actin-1. In PHHs, CLD at 5 μM for 24 h also decreased SEPT2 and SEPT7 abundance by 38 % and 35 %, respectively, whereas no variation was reported for CLDOH at 10 μM after 24 h (Fig. 3D, Fig. 4C). We further investigated the mechanism responsible for the decrease in septins following CLD exposure. As the abundance of septins decreased rapidly (from 8 h of treatment), we expected a degradation process rather than a decrease in septin expression. Therefore, the impact of CLD on septins was investigated with two degradation inhibitors: bafilomycin A1 (Baf), an inhibitor of vacuolar ATPase and lysosome degradation, and MG132, an inhibitor of proteasome degradation. MG132 induced higher abundance in heat shock proteins such as HspA1B, HspB1 and HspH1 (Supplementary Fig. S7A) indicating the effectiveness of the treatment, given that MG132 generally causes an up-regulation of heat shock proteins in human cells [52]. The decrease in septin abundance induced by CLD was not affected with the addition of Baf, and it was more or less annulled with MG132 (Fig. 4D, supplementary Fig. S7B). Two-way ANOVA p-values revealed that an interaction was observed for septins by a co-treatment of CLD with MG132, whereas no effect was reported for MG132 alone (Supplementary File S2). Violin plots confirmed that the degradation of Septin-2, − 7, − 9, − 10, and − 11 induced by CLD occurred by proteasomal degradation instead of vacuolar degradation (Fig. 4E). Indeed, MG132, but not Baf, was able to largely abolish the decrease in septin abundance induced by CLD exposure, suggesting the involvement of proteasomal degradation. To note, ubiquitin signatures (residues GG on lysines) were not identified for septins in the proteomic datasets. Moreover, no signatures of proteasomal degradation were detected in the proteomic datasets when searching for specific cleavage sites other than lysine or arginine (meaning other trypsin specificity) in the proteomic database search engine.

Although no difference in toxicity could be detected when MG132 was added to CLD compared with CLD alone after 5 h of exposure, a slight decrease was observed after 24 h, suggesting that proteasomal degradation was involved in CLD toxicity (Fig. 4F). Such a decrease in toxicity when adding MG132 was not observed with CLDOH, which did not induce proteasomal degradation of septins and was less cytotoxic than CLD. It should be noted that MG132 potentiated CLD and CLDOH cytotoxicity after 48 h of exposure (Supplementary Fig. S8). Among all quantified proteins, septins are the main proteins affected by CLD and MG132 exposures (Fig. 4D). Therefore, the partial rescue of septin degradation induced by MG132 is probably involved in the protection of CLD cytotoxicity (Fig. 4F).

3.6. Binding of CLD and CLDOH to septins

Molecular interaction between CLD or CLDOH and septins was investigated by molecular docking (Fig. 5A). Affinities (kcal/mol) for septins of different ligands were tested and compared. Forchlorfenuron, a known agonist of Septin-2, − 3, and − 7 interacting in the GDP domain, was used as a positive control. The chlorinated pesticide tebufenpyrad (TEBU) was used as a negative control according to previous results (Léger et al., 2023). GDP alone was used as an internal control for molecular docking. Affinities of interaction with SEPT2 were − 7.459 and − 7.249 for CLD and CLDOH, respectively. Similar affinities were observed with the TEBU control (Supplementary Table S2). Except for TEBU, interactions occurred in SEPT2's GDP domain. Septin affinities for CLD and CLDOH were higher than those obtained for GDP and forchlorfenuron, compounds known to bind septins, indicating potential interaction between CLD or CLDOH and septins. Moreover, the interaction of recombinant SEPT2 with CLD and CLDOH was confirmed by SPR, whereas no interaction was observed with TEBU and tamoxifen (Fig. 5B). Forchlorfenuron, a pesticide described as interacting with septins, showed no affinity for SEPT2 by SPR.

3.7. CLD impaired size and distribution of lipid droplets (LDs) as well as septin polymerization

In order to clarify whether CLD's impact on septins can affect LDs, they were visualized in HepaRG cells using an ArrayScan high-content screening (HCS) system. In both control and CLDOH-treated cells, the labeling of neutral lipids revealed large perinuclear LDs whereas, small, dispersed and dense LDs were found in CLD-treated cells (Fig. 5C), without any change in the total amount of neutral lipids (Fig. 5D). Unlike CLDOH, the decrease in SEPT2 and SEPT9 abundance highlighted by proteomics and confirmed by HCS (Fig. 5D) led to depolymerization of septin filaments visualized by HCS following CLD exposure (Fig. 5C). Lysosomes (Lamp-1 labeling), which interplay with LDs in lipophagy, and F-actin fibers (phalloidin labeling) did not change following CLD and CLDOH exposure. Similarly, proteomic analyses did not show an effect on proteins associated with lysosomes such as LAMP-1, MACP2, PRCP, SCARB2, MAN2B, and GAA (Supplementary File S2).

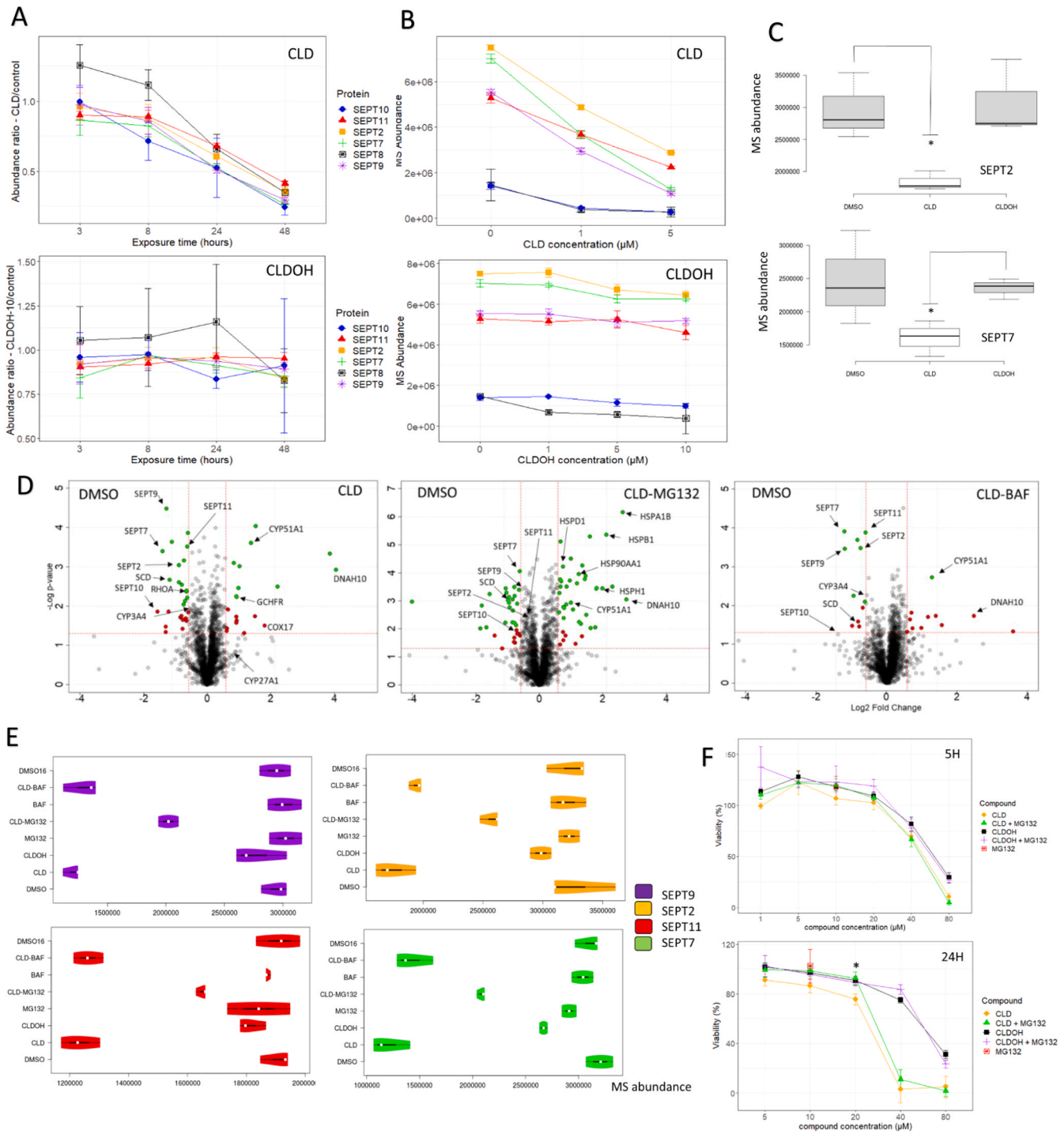

Fig. 4. Impact of CLD and CLDOH treatment on septin abundance and degradation. (A) Time variations of septin abundance in HepaRG cells after 3, 8, 24, and 48 h of CLD (5 µM, top panel) and CLDOH (10 µM, bottom panel) exposure. The corresponding volcano plots are presented in Supplementary Fig. S5. (B) Septin abundance variations in HepaRG cells following CLD (1, 5 µM, top panel) and CLDOH (1, 5, 10 µM, bottom panel). The full proteomic dataset is presented in Supplementary File S2. (C) Boxplots showing abundance variations of Septin-2 and − 7 in PHHs obtained by proteomics. (D) Volcano plots representing protein abundance variations following co-exposure of CLD (5 µM) or CLDOH (10 µM) with bafilomycin (10 nM) or MG132 (10 µM) for 24 h. Protein degradation was investigated using MG132, an inhibitor of proteasomal degradation and bafilomycin (Baf), an inhibitor of lysosomal degradation. P-values were calculated using two-sided Student's t-tests. Red dots represent proteins with p-values between 0.01 and 0.05, and a fold change greater than 1.5. Green dots represent proteins with p-values lower than 0.01, and a fold change greater than 1.5. The full dataset is presented in Supplementary File S2. (E) Violin plots representing normalized abundance values of septins in HepaRG cells following CLD, CLDOH, MG132, and Baf exposure. The DMSO and DMSO16 correspond to solvent controls containing 0.1 % and 0.16 % DMSO, respectively. (F) Trendlines showing HepaRG cell viability following 5 and 24 h exposure to CLD and CLDOH (5, 10, 20, 40, 80 µM) with or without MG132 (10 µM). Biological triplicates were used for each experiment. Viability was significantly increased following CLD-MG132 exposure (20 µM for 24 h) compared with CLD exposure.

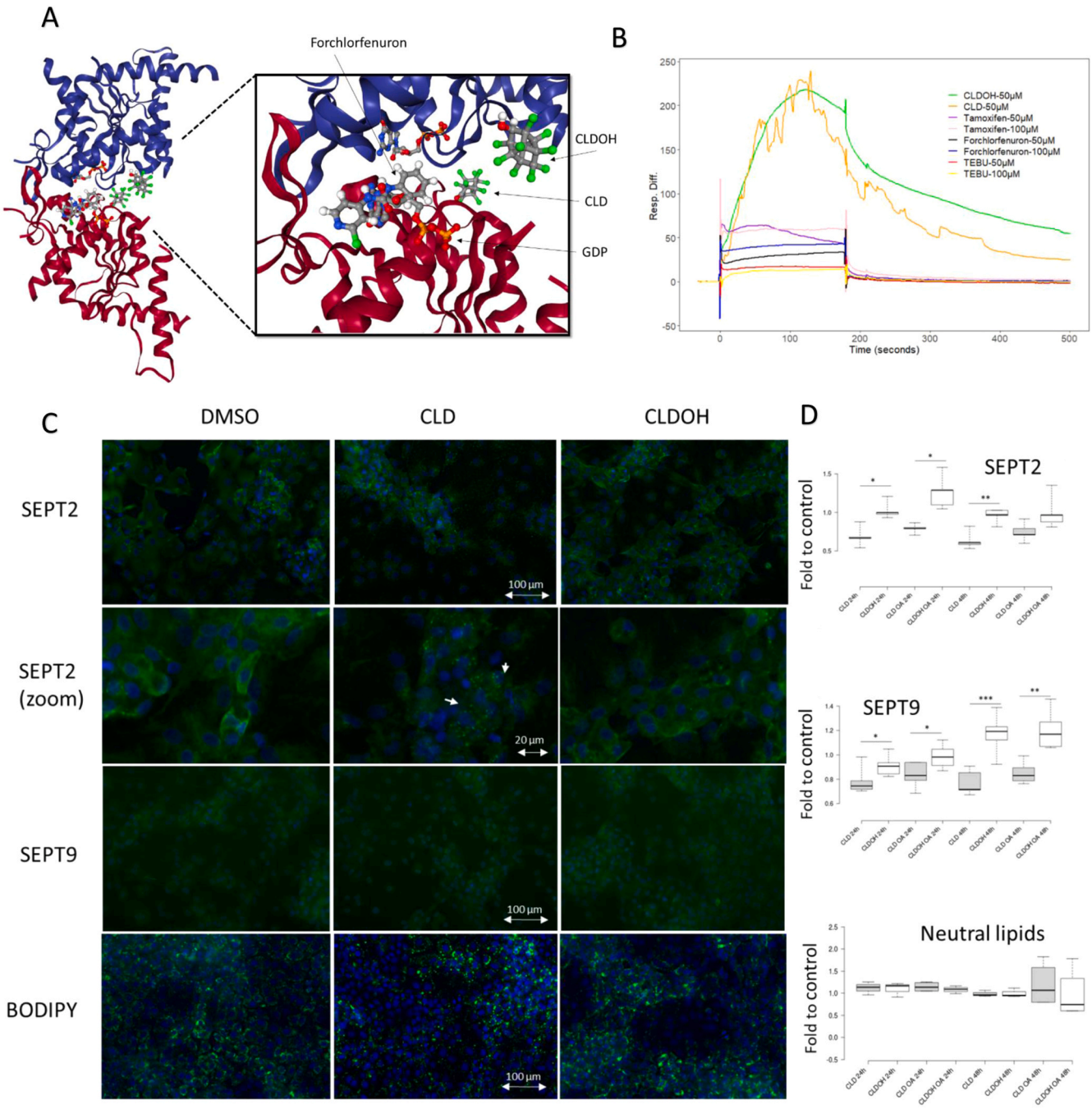

Fig. 5. Septin interaction with CLD and impact of CLD on the size of lipid droplets. (A) 3D structures of CLD, CLDOH, forchlorfenuron, and GDP interactions with SEPT2 obtained by blind molecular docking. Affinities are indicated in Supplementary Table S2. (B) Surface plasmon resonance analyses showing interactions of CLD and CLDOH with SEPT2. TEBU, tamoxifen and forchlorfenuron were used as controls. (C) Representative images of SEPT2 and SEPT9 in HepaRG cells following CLD (5 µM) and CLDOH (10 µM) 48 h exposures measured by high-content screening (HCS). LD location after CLD and CLDOH exposure, detected by HCS using BODIPY labeling, is also shown. (D) Boxplots showing SEPT2, SEPT9 and neutral lipids (BODIPY) abundance measured by HCS in HepaRG cells following CLD and CLDOH exposure (OA: oleic acid).

3.8. CLD and to a lesser extent CLDOH increased production and secretion of saturated long-chain DCAs

Metabolomics indicated that HepaRG cell content in phospholipids (steaoryl-GPE, palmitoyl-GPE, oleoyl-GPE, arachidonyl-GPE) and saturated or unsaturated fatty acids (such as palmitic (C16), stearic (C18), linoleic (C18), oleic (C18), hydroxystearic (C18), and hydroxyarachidic (C20) carboxylic acids) did not vary after CLD and CLDOH treatment (Fig. 6A). However, following CLD exposure, saturated long-chain DCAs such as tetra- (C14), methyltetra- (C15), penta- (C15), and hepta- (C17) decanedioic fatty acids increased in cell culture medium (Fig. 6B, Fig. 6C) and in cell content (Fig. 6B, Supplementary Fig. S9A). A smaller increase was also observed in the same DCAs following CLDOH exposure in cell culture medium and cell content. In contrast, both intra- and extra-cellular levels of C16-DCA hexadecanedioic acid decreased after 48 h of exposure to CLD (respective ratios of 0.57 and 0.33) and CLDOH (respective ratios of 0.77 and 0.46). No statistical variation in short DCAs such as glutaric acid (C5), adipic acid (C6), pimelic acid (C7), succinic acid (C8), sebacic acid (C10), dodecanedioic acid (C12), and brassylic acid (C13) was observed in cell culture media after CLD and

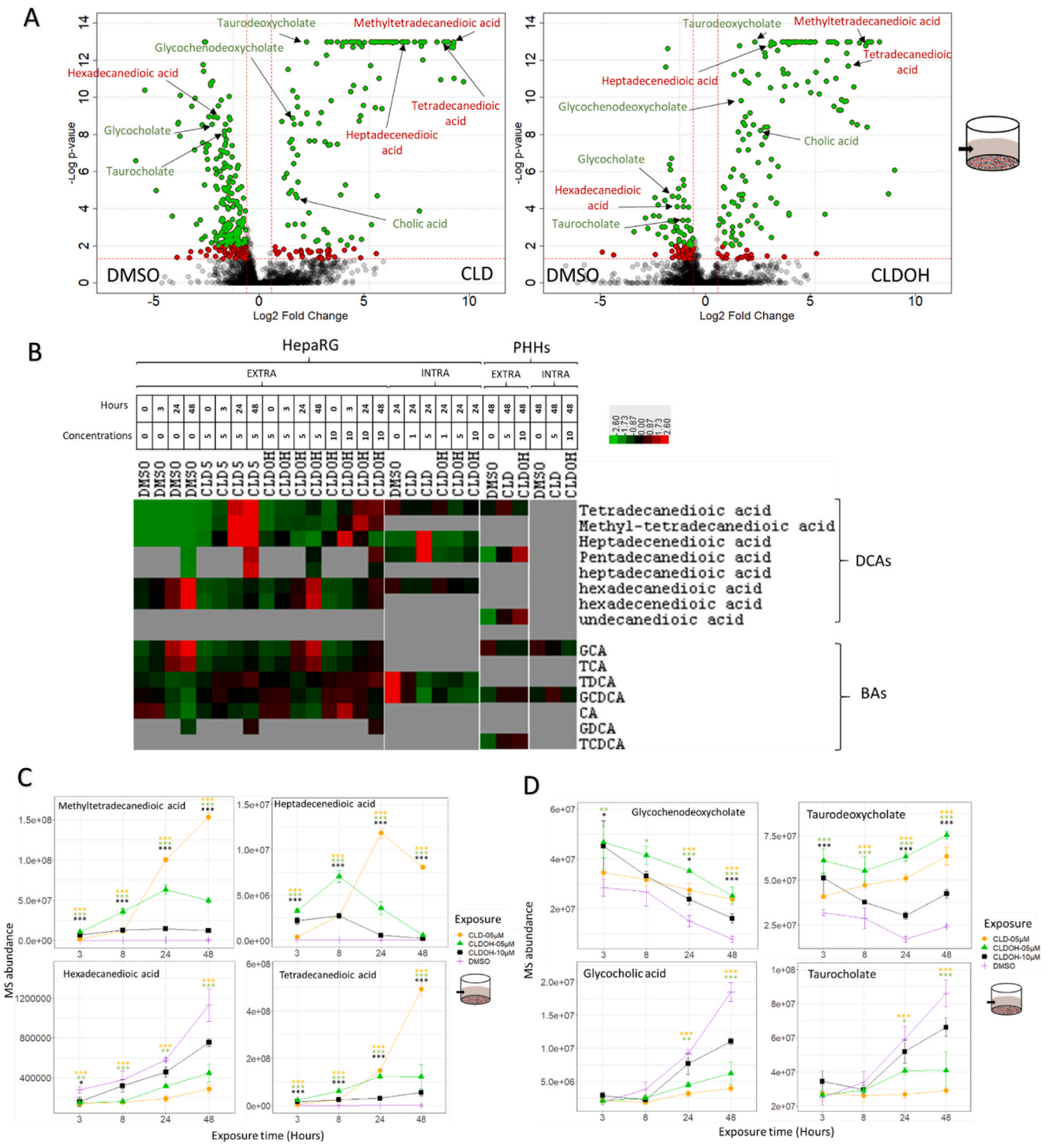

Fig. 6. Impact of CLD and CLDOH on content and secretion of bile acids and saturated long-chain dicarboxylic acids in hepatic cell models. (A) Volcano plots showing variations in the abundance of extracellular metabolites from HepaRG cell culture following exposure to CLD (5 µM) and CLDOH (10 µM). (B) Heatmap showing the variations in DCA and BA abundance induced in HepaRG cells and PHHs by CLD and CLDOH exposure. The reported values are abundance values normalized by means. Complete datasets are presented in Supplementary File S5 and Supplementary File S6. (GCA: glycocholic acid, TCA: taurocholic acid, TDCA: taurodeoxycholic acid, GCDCA: glycochenodeoxycholic acid, CA: cholic acid, GDCA: glycodeoxycholic acid, TCDCA: taurochenodeoxycholic acid). (C) Trendline charts showing the variations in saturated long-chain DCA abundance in HepaRG cell culture media following exposure to CLD (5 µM) and CLDOH (5, 10 µM). For statistical tests, each exposure condition was compared to the solvent (DMSO) control. (D) Trendline charts showing the variations in BA abundance in HepaRG cell culture media following exposure to CLD (5 µM) and CLDOH (5, 10 µM). For statistical tests, each exposure condition was compared to the solvent (DMSO) control.

CLDOH treatment. Extracellular levels of undecanedioic acid (C11) and certain long-chain saturated DCAs increased in PHHs treated by CLD (Supplementary Fig. S9B). It must be emphasized that very-long-chain DCAs (C>22) were not identified in our metabolomic datasets. Concomitant to this increase in saturated DCAs, CLD but not CLDOH decreased the level of the stearoyl-CoA 9-desaturase (SCD) protein, which is essential for fatty acid desaturation and lipid storage in HepaRG cells (Fig. 4D, Supplementary Fig. S6A). However, this decrease did not seem to be due to either proteasomal or vacuolar degradation, in line with the absence of MG132 and bafilomycin effects (Supplementary Fig. S6B).

3.9. CLD and CLDOH perturbed BA production and secretion

BA production and secretion were disrupted by CLD and CLDOH (Fig. 6A, Fig. 6B). Indeed, a drastic decrease (between 42 % and 74 %) in the secretion of conjugated primary BAs such as glycocholic (GCA) and taurocholic acids (TCA) was observed following CLD and CLDOH exposure (5 μM and 10 μM, respectively, 48 h) (Fig. 6D). In contrast, the extracellular level of taurodeoxycholic (TDCA) and glycochenodeoxycholic (GCDCA) acids increased by a factor of around 2.6 and 3 following 48-hour exposure to CLD and CLDOH, respectively. TDCA decreased in HepaRG cell content (factors of 7.2 and 6.1, respectively) following CLD and CLDOH exposure (Supplementary Fig. S9C), indicating an increase in its secretion. The amount of GCDCA in cell content decreased 20- and 8.3-fold, respectively, after 24 h of treatment with CLD and CLDOH (Fig. 6B, Supplementary Fig. S9C), but concomitantly increased in cell culture media (Fig. 6D). This indicated that secretion increased, exceeding production. TDCA abundance varied like that of GCDCA in cell culture medium and HepaRG cell content. For PHHs, the abundance of taurochenodeoxycholic (TCDCA) and GCDCA acids increased in cell culture medium following exposure to CLD (by factors of 4.3 and 2.4, respectively) and CLDOH (4.7 and 2.3, respectively) (Supplementary Fig. S9D). In contrast, like HepaRG cells, GCA abundance decreased by factors of, respectively, 1.9 (CLD, 5 μM, 48 h) and 1.9 (CLDOH, 10 μM, 48 h) (Supplementary Fig. S9D). The abundance of intracellular GCA in PHHs decreased by factors of 1.3 and 2.4, respectively, following CLD and CLDOH exposure. The abundance of intracellular GCDCA increased by factors of 2.8 (CLD, 48 h) and 2 (CLDOH, 48 h), indicating an increase in its production and secretion like HepaRG cells (Supplementary File S5, Supplementary File S6). Cyp51A1, implicated in bile acid metabolism and cholesterol synthesis from lanosterol and acetyl-CoA, increased following CLD exposure (Fig. 3A, Fig. 4D).

3.10. CLD but not CLDOH induced fibrosis in liver organoids modelling MASLD

A liver organoid model containing hepatocytes and biliary cells (HepaRG cell line), stellate cells (LX-2 cell line) and human primary macrophages was used to investigate the impact of CLD and CLDOH on healthy and fat-overloaded organoids (Fig. 7A). In healthy organoids, CLD and CLDOH showed the same cytotoxic response while a fat overload reduced cytotoxicity (Fig. 7B). Indeed, IC50 values for CLD and CLDOH were 6.4 and 5.39 μM, respectively, in healthy organoids and 12.8 and 19.16 μM in organoids with a fat overload. CLD and CLDOH exposure induced a similar IL-6 release by healthy organoids (Fig. 7C, top panel), whereas the increase was lower in steatotic (with pre-existing inflammation) organoids (Fig. 7C, bottom panel). It should be mentioned that no induction of IL-6 release was observed in 2D HepaRG cells following CLD and CLDOH exposure (Supplementary Fig. S10), suggesting that the IL-6 release observed in HML organoids could be due to macrophages. No induction (Fig. 7D, top panel) or exacerbation (Fig. 7D, bottom panel) of steatosis was observed for CLD and CLDOH after 7 days of exposure (Supplementary Fig. S11). Fibrosis was evaluated in the organoids through labeling of vimentin (as a marker for stellate cells) and quantification of collagen 1 (COL1) and collagen 4 (COL4) immunofluorescence (Fig. 7E, Supplementary Fig. S12). Image analysis of COL1 (in red) and COL4 (in yellow) shows that both markers colocalize in all the tested conditions. An increase in the amount of COL1 and COL4 suggested that CLD but not CLDOH was able to trigger fibrosis without inducing a fat overload (Fig. 7F, top panel, Supplementary Fig. S13A). However, a decrease of fibrosis was observed following CLD and CLDOH exposures coupled with a fat overload comparatively to the control condition with fat overload (Fig. 7F, bottom panel, Supplementary Fig. S13B).

4. Discussion

In this study, we aimed to decipher the cellular effects induced by CLD and its major metabolite CLDOH on human liver cells, as well as their potential involvement in MASLD susceptibility. HepaRG is currently the most widely accepted cellular model for studying the metabolism and hepatotoxicity of xenobiotics such as drugs, chemicals, and pesticides. Indeed, this human cell line expresses liver-specific functions at high levels, particularly phase I and phase II biotransformation enzymes [53]. In addition, together with non-parenchymal cells, HepaRG can form multicellular organoids able to mimic various pathological situations such as fibrosis and MASLD [44]. Although liver cells were more sensitive to CLD than CLDOH in the MTT assay, both compounds induced a slight and comparable decrease in ATP levels in HepaRG cells, returning to normal after 24 h. Probably to compensate for this ATP decrease, the abundance of OXPHOS components slightly increased after CLD and CLDOH treatment, without any effect on ROS level. Therefore, due to the slight decrease and rapid compensation observed, the impact of CLD and CLDOH on the ATP level is not likely to be the major mechanism leading to hepatotoxicity.

As expected, CLD was metabolized more slowly than CLDOH and remained at high concentrations in hepatocytes, indicating liver sequestration as demonstrated by pharmacokinetic modeling based on data from rats and monkeys [35]. Secreted metabolites were mainly glucuronides as previously described for exposed workers [15]. CLDOH was massively and rapidly converted into glucuronide forms found in the extracellular medium, demonstrating efficient transformation by phase II enzymes and efflux by phase III transporters in HepaRG cells and PHHs. In contrast, CLD did not convert well to CLDOH and then CLDOH-G. The abundance of AKR1C4, the main enzyme that converts CLD into CLDOH, was unaffected in HepaRG cells.

Among its pleiotropic effects, CLD was described as disrupting adherens junctions, decreasing proteins E-cadherin and beta-catenin in human breast epithelial cells, both of which neighbor the actin cytoskeleton [54]. While both CLD and CLDOH induced a slight variation in beta-catenin, CLD greatly decreased some cytoskeletal proteins such as Septin-2, − 7, − 9, − 10, and − 11 in HepaRG cells, and Septin-2 and − 7 in PHHs. Septins are highly conserved eukaryote GTPases (with a Mg^{2+} cofactor) and are considered the fourth cytoskeleton component [55]. Among the 13 septins described in humans, SEPT7 has been reported to be the one mostly involved in the cytoskeleton and triggering degradation of other septins [56]. Except Septin-1, − 3, − 12, and − 14, which are expressed in specific tissue, the others are widely expressed in organs [57]. They polymerize into filaments forming homo and hetero-oligomeric structures with preferential association of forms [55, 58]. Septins are implicated in intracellular vesicular trafficking, cellular signaling and cell migration [56], and regulate actin and microtubule organization [59]. Using degradation inhibitors, we showed that proteasomal degradation was likely involved in the drastic decrease in septins induced by CLD. Moreover, no covalent protein adducts of CLD—notably by the formation of hemithioketals [35]—and no ubiquitination and proteolytic signatures of septin degradation were detected in our proteomic datasets. Septins were also shown to affect cell cycles. SEPT7 has been described as controling S-phase entry and orchestrating microtubule nucleation arrays [60], while, in mouse and yeast, its deletion has been associated with a destabilization of

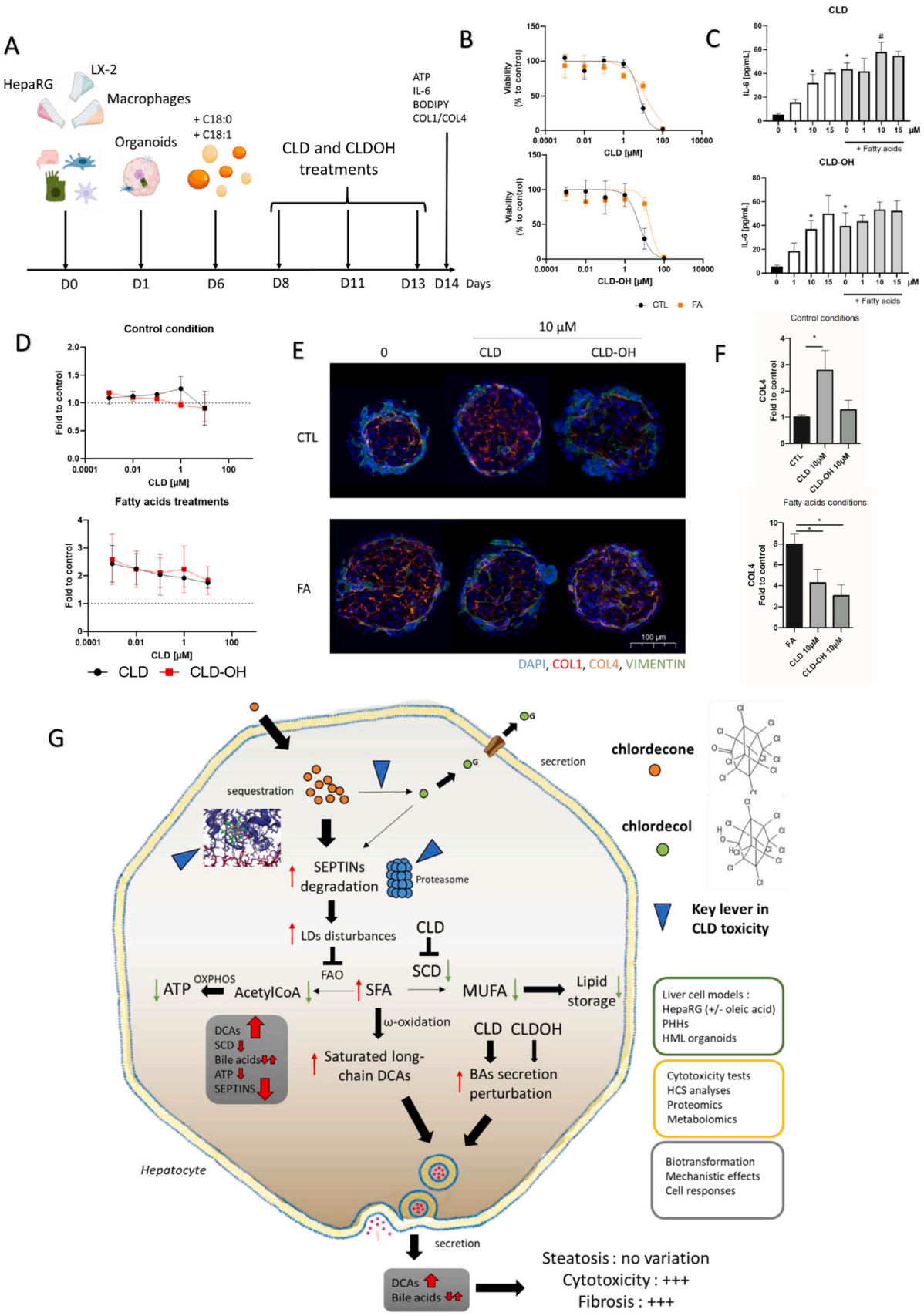

(caption on next page)

Fig. 7. Mechanisms associated with CLD-induced hepatotoxicity and susceptibility to MASLD. (A) Diagram showing the exposure protocol of the 3D MASLD liver model to CLD and CLDOH. (B) Cytotoxicity induced by CLD and CLDOH exposure on the liver model of MASLD. (C) Quantification of IL-6 release by immunofluorescence in cell culture media of the 3D liver model repeatedly exposed to CLD and CLDOH. (D) Quantification of steatosis on the liver model of MASLD exposed to repeated doses of CLD and CLDOH. Neutral lipids and lipid droplets were labeled with BODIPY to quantify steatosis. (E) Vizualisation by immunofluorescence and confocal microscopy of fibrosis in the 3D liver model repeatedly exposed to CLD and CLDOH. Collagen 1 (COL1), collagen 4 (COL4), and vimentin were labeled and visualized. DAPI was used to label nuclei. (F) Quantification of COL4 abundance in control and fatty organoids (n = 3). Quantification of COL1 is presented in the supplementary Fig. S13. (G) Proposed model for CLD-induced hepatotoxicity and susceptibility to MASLD including remediation strategies that could be proposed: converting CLD to CLDOH, targeting proteasome degradation or using CLD's affinity for septins. All the observed effects are summarized in Supplementary Table S3. (MUFA: monounsaturated fatty acids, SFA: saturated fatty acids).

microtubules and cytokinesis completion [61]. SEPT6 deletion has also been reported to inhibit proliferation and cell cycle progression and promote apoptosis [62]. Variations in abundance and deletion of septins [56] such as SEPT 7, 9, or 11 [57] have been related to various cancers. Mutations of septins in the GTP-binding pocket have been associated with skin, stomach, and large intestine cancers [63]. Moreover, up-regulation of SEPT2, 8, and 9, and down-regulation of SEPT4 and SEPT10 have been shown in many cancers, including liver cancer [64]. In contrast, SEPT2 and SEPT9 repression has been associated with tumor growth suppression in human glioblastoma cells [65]. The involvement of septins in triggering liver fibrosis has been proven but the process remains unclear. Indeed, loss of SEPT4 has exacerbated liver fibrosis in mice [66] whereas an increase in SEPT4 and SEPT6 [62] and decrease in SEPT9 [67] have been described in in vivo models of liver fibrosis.

Interaction of septins with CLD could explain their proteasomal degradation, as the ubiquitin proteasome system targets misfolded and damaged proteins. Molecular docking indicated a potential interaction of CLD and CLDOH with the GDP-binding domain of septins, close to the Mg^{2+} cofactor binding site. Interactions of CLD and CLDOH with SEPT2 were confirmed by SPR. A binding mechanism similar to that of forchlorfenuron, a chlorinated pesticide able to destabilize septin assembly and organization [68], and reacting with the GDP-binding domain of septins [69], could be suggested. Although molecular docking and SPR concluded that there was a high affinity between CLDOH and septins, the quick metabolization of CLDOH compared with CLD likely prevents CLDOH and septin interaction, and consequently septin degradation.

We showed that the impact of CLD on septin degradation resulted in a decrease in LD size and a decrease in SCD abundance, which is essential for the formation of large LDs [70]. In mouse liver, CLD was also reported to decrease the number of LDs [71]. Moreover, SEPT9 was shown to promote a perinuclear location of LDs in COS-7 cells [72] and Huh7 cells [73] and to induce LD growth [74]. Dysregulation of LD biogenesis can result in ER stress, inflammation and then MASLD [75]. Indeed, in microvesicular steatosis, LDs are redistributed due to severe FAO inhibition and lipolysis [76,77]. The disruption of LD size induced by CLD impacted fatty acid metabolism by increasing saturated long-chain DCA production and secretion, and by disrupting BA secretion. It should be noted that PHHs and HepaRG cells appeared to try to limit the synthesis of DCAs following CLD exposure by reducing the abundance of CYP3E4 and CYP2E1, oxidases implicated in their production [78]. In contrast, CLD did not affect the content of free fatty acids (FFA) intended for beta-oxidation or esterified for triglyceride storage. However, the amount of some carboxylic acids changed, as previously shown in mouse liver [71]. Perturbation of the hepatic lipid metabolism has been reported in the context of MASLD progression [3]. High levels of long-chain DCAs and bile acids have been observed in the serum of cirrhotic patients [79]. The presence of DCAs with more than 10 to 12 carbons is a signature of mitochondrial FAO deficiency [80], which has been shown to be associated globally with MASLD [81,82] and MASLD severity in humans [83]. Indeed, long-chain DCAs are more toxic than carboxylic acids and can induce steatohepatitis if peroxisomal beta oxidation is not efficient [84]. Moreover, the impaired contact of LDs with mitochondria was seen to reduce FAO and could lead to progression of MASLD in rats [85]. We demonstrated that SCD abundance decreased following CLD exposure, favoring the production of saturated fatty acids, generally dedicated to FAO, instead of monounsaturated fatty acids more commonly associated with triglyceride storage. The resulting inhibition of FAO combined with a decrease in SCD abundance could further explain the increase in saturated long-chain DCAs toxic for hepatocytes and produced by ω-oxidation. Indeed, SCD-/- mice have shown a decrease in steatosis and a rise in steatohepatitis [86], whereas an increase in SCD has been reported in steatosis models induced by amidarone and tetracycline [87].

Following treatment of liver cells with CLD and, to a lesser extent with CLDOH, we showed that BA production and abundance were affected, with increased secretion of taurodeoxycholic, glycochenodeoxycholic, and cholic acids and decreased secretion of taurocholic and glycocholic acids. A decreased secretion of taurocholate has also been observed in rat liver following CLD exposure in vivo [88]. BAs, synthetized from cholesterol in the liver, are major constituants of bile and changes to their amount and composition have been implicated in the progression of MASLD in rodents and humans [89,90]. Moreover, alteration of BA synthesis and circulation has been reported in MASLD [91,92] and an increase in serum levels of glycocholic, taurocholic, and glycochenodeoxycholic acids has been described in patients with NASH compared with healthy individuals [93]. We showed that CYP51A1, an important enzyme for BA synthesis from cholesterol, was up-regulated following CLD exposure, as reported in NASH-HCC mice [94], while CYP3A4, which detoxifies excess BAs, decreased, as previously reported in MASLD and NASH in humans [95]. Mutations of AKR1C4 have been reported to induce BA deficiency [96]. This enzyme is also implicated in CLD metabolism, converting CLD into CLDOH. Saturation of AKR1C4 activity due to CLD exposure could explain the perturbation observed in BA production and secretion.

Furthermore, the results obtained with MASLD organoid models exposed to CLD and CLDOH confirmed the greater potentiating effect of CLD in the progression of liver disease by increasing fibrosis without fat overload. A similar outcome has been reported in mouse liver after co-treatment by CLD and carbon tetrachloride [30]. To note, an inverse association between plasma chlordecone concentrations and progression of liver alcoholic fibrosis was recently described in an epidemiological study [97]. We also found a slight decrease in fibrosis in organoids with fat overload following CLD and CLDOH exposures, suggesting that MASLD may not be an additional risk factor for CLD hepatotoxicity. We showed that the interaction of CLD with septins induced their degradation, a key event in hepatoxicity and fibrosis development and progression. No effect of CLDOH in the MASLD model was observed, probably because it was too quickly metabolized to interact with septins, as shown in HepaRG cells. We revealed that specific effects of CLD—such as septin degradation, an increase in saturated long-chain DCA production and secretion, perturbation of BAs and a decrease in SCD abundance—are key mechanisms implicated in liver fibrosis development (Fig. 7G, Supplementary Table S3). The implication of these results on HCC remains to be studied even though, contrary to prostate cancer, the prevalence of liver cancer has proved to be lower in FWI than in metropolitan France (Santé publique France, 2019).

Facing the urgent need to develop therapies for limiting CLD toxicity [98] and susceptibility to fibrosis, this study also highlighted that inhibiting septin degradation, utilizing CLD's affinity for septins and promoting the conversion of CLD to CLDOH could be effective strategies. Further studies will be carried out to determine whether the observed mechanisms of action of CLD can be generalized to other cell types or

organs including the liver, given that septins are ubiquitously expressed, and to provide mechanistic clues as to the potential involvement of CLD in other pathologies.

Environmental implication

Chlordecone is an organochlorine insecticide used from 1972 to 1993 to control the banana weevil. Because of its persistence in soil, its presence in 2014 in 95 % of the population of the French West Indies despite its ban and its implication in various pathologies such as prostate cancer, the CLD is the subject of various remediation strategies in food and soil. Our work has indicated, using in vitro liver cells models, the potential benefits of increasing the conversion of CLD into CLDOH, a process occurring weakly in humans, on human health and particularly on hepatotoxicity and fibrosis.

CRediT authorship contribution statement

Yoann Devriendt-Renault: Validation, Resources, Methodology, Formal analysis. **Sylvie Huet:** Validation, Resources, Methodology, Formal analysis. **Rachelle Lanceleur:** Visualization, Validation, Resources, Methodology, Formal analysis. **Ludovic Le Hégarat:** Writing – review & editing, Resources, Methodology, Investigation, Formal analysis, Conceptualization. **Thibaut Léger:** Writing – review & editing, Writing – original draft, Visualization, Validation, Supervision, Software, Resources, Project administration, Methodology, Investigation, Formal analysis, Data curation, Conceptualization. **Valérie Fessard:** Writing – review & editing, Methodology, Investigation, Conceptualization. **Bruno Clément:** Writing – review & editing, Investigation, Conceptualization. **Julien Parinet:** Resources, Investigation, Conceptualization. **Tahar Bouceba:** Visualization, Validation, Software, Resources, Methodology, Formal analysis. **Léonie Dec:** Software, Formal analysis, Data curation. **Pierre-Jean Ferron:** Visualization, Validation, Software, Resources, Methodology, Investigation, Formal analysis. **Sarah Alilat:** Writing – review & editing, Visualization, Software, Methodology, Investigation, Formal analysis, Data curation.

Declaration of Competing Interest

None of the authors have any conflict of interest.

Data availability

Proteomic datasets are available in the PRIDE partner repository and Metabolomic data are available in the Metabolights repository. The identifiers are provided in the article.

Acknowledgments

The authors are grateful to Anne-Louise Blier, Kevin Hogeveen (Fougères Laboratory, French Agency for Food, Environmental and Occupational Health & Safety (ANSES)) for their technical support. We thank Delphine Libby-Claybrough (Coup de Puce Expansion) for correcting the English version of this text.

Appendix A. Supporting information

Supplementary data associated with this article can be found in the online version at doi:10.1016/j.jhazmat.2024.135177.

References

[1] Riazi, K., Azhari, H., Charette, J.H., Underwood, F.E., King, J.A., Afshar, E.E., et al., 2022. The prevalence and incidence of NAFLD worldwide: a systematic review and meta-analysis. Lancet Gastroenterol Hepatol 7, 851–861.
[2] Juanola, O., Martinez-Lopez, S., Frances, R., Gomez-Hurtado, I., 2021. Non-alcoholic fatty liver disease: metabolic, genetic, epigenetic and environmental risk factors. Int J Environ Res Public Health 18.
[3] Sen, P., Qadri, S., Luukkonen, P.K., Ragnarsdottir, O., McGlinchey, A., Jantti, S., et al., 2022. Exposure to environmental contaminants is associated with altered hepatic lipid metabolism in non-alcoholic fatty liver disease. J Hepatol 76, 283–293.
[4] Cave, M., Falkner, K.C., Ray, M., Joshi-Barve, S., Brock, G., Khan, R., et al., 2010. Toxicant-associated steatohepatitis in vinyl chloride workers. Hepatology 51, 474–481.
[5] Benharroch, D., Talalay, B., 2017. Toxicant-associated steatohepatitis: a propos a case of benzene exposure. Int Med Case Rep J 10, 73–75.
[6] Deierlein, A.L., Rock, S., Park, S., 2017. Persistent endocrine-disrupting chemicals and fatty liver disease. Curr Environ Health Rep 4, 439–449.
[7] Wahlang, B., Beier, J.I., Clair, H.B., Bellis-Jones, H.J., Falkner, K.C., McClain, C.J., et al., 2013. Toxicant-associated steatohepatitis. Toxicol Pathol 41, 343–360.
[8] Haug, K., Cochrane, K., Nainala, V.C., Williams, M., Chang, J., Jayaseelan, K.V., et al., 2020. MetaboLights: a resource evolving in response to the needs of its scientific community. Nucleic Acids Res 48, D440–D444.
[9] Perez-Riverol, Y., Bai, J., Bandla, C., Garcia-Seisdedos, D., Hewapathirana, S., Kamatchinathan, S., et al., 2022. The PRIDE database resources in 2022: a hub for mass spectrometry-based proteomics evidences. Nucleic Acids Res 50, D543–D552.
[10] Sang, H., Lee, K.N., Jung, C.H., Han, K., Koh, E.H., 2022. Association between organochlorine pesticides and nonalcoholic fatty liver disease in the National Health and Nutrition Examination Survey 2003-2004. Sci Rep 12, 11590.
[11] Devault, D.A., Laplanche, C., Pascaline, H., Bristeau, S., Mouvet, C., Macarie, H., 2016. Natural transformation of chlordecone into 5b-hydrochlordecone in French West Indies soils: statistical evidence for investigating long-term persistence of organic pollutants. Environ Sci Pollut Res Int 23, 81–97.
[12] Dereumeaux, C., Saoudi, A., Guldner, L., Pecheux, M., Chesneau, J., Thome, J.P., et al., 2020. Chlordecone and organochlorine compound levels in the French West Indies population in 2013-2014. Environ Sci Pollut Res Int 27, 41033–41045.
[13] Resiere, D., Florentin, J., Kallel, H., Banydeen, R., Valentino, R., Drame, M., et al., 2023. Chlordecone (Kepone) poisoning in the French Territories in the Americas. Lancet 401, 916.
[14] Cohn, W.J., Boylan, J.J., Blanke, R.V., Fariss, M.W., Howell, J.R., Guzelian, P.S., 1978. Treatment of chlordecone (Kepone) toxicity with cholestyramine. Results of a controlled clinical trial. N Engl J Med 298, 243–248.
[15] Guzelian, P.S., 1981. Therapeutic approaches for chlordecone poisoning in humans. J Toxicol Environ Health 8, 757–766.
[16] ANSES (2021). Valeurs sanitaires de référence: le chlordecone. Avis de l'Anses, Saisine n° " 2018-SA-0166 ".
[17] DREES-Insee, 2019. Premiers résultats de l'enquête santé européenne, 2021. EHIS.
[18] EPA (2009). TOXICOLOGICAL REVIEW OF CHLORDECONE (KEPONE). EPA/635/R-07/004F.
[19] Santé publique France, Indc (2019). Estimations régionales et départementales d'incidence et de mortalité par cancers en France, 2007–2016.
[20] Multigner, L., Kadhel, P., Rouget, F., Blanchet, P., Cordier, S., 2016. Chlordecone exposure and adverse effects in French West Indies populations. Environ Sci Pollut Res Int 23, 3–8.
[21] Multigner, L., Ndong, J.R., Giusti, A., Romana, M., Delacroix-Maillard, H., Cordier, S., et al., 2010. Chlordecone exposure and risk of prostate cancer. J Clin Oncol 28, 3457–3462.
[22] Cordier, S., Bouquet, E., Warembourg, C., Massart, C., Rouget, F., Kadhel, P., et al., 2015. Perinatal exposure to chlordecone, thyroid hormone status and neurodevelopment in infants: the Timoun cohort study in Guadeloupe (French West Indies). Environ Res 138, 271–278.
[23] Oulhote, Y., Rouget, F., Michineau, L., Monfort, C., Desrochers-Couture, M., Thome, J.P., et al., 2023. Prenatal and childhood chlordecone exposure, cognitive abilities and problem behaviors in 7-year-old children: the TIMOUN mother-child cohort in Guadeloupe. Environ Health 22, 21.
[24] Gaudriault, P., Mazaud-Guittot, S., Lavoue, V., Coiffec, I., Lesne, L., Dejucq-Rainsford, N., et al., 2017. Endocrine disruption in human fetal testis explants by individual and combined exposures to selected pharmaceuticals, pesticides, and environmental pollutants. Environ Health Perspect 125, 087004.
[25] Hammond, B., Katzenellenbogen, B.S., Krauthammer, N., McConnell, J., 1979. Estrogenic activity of the insecticide chlordecone (Kepone) and interaction with uterine estrogen receptors. Proc Natl Acad Sci USA 76, 6641–6645.
[26] Lemaire, G., Mnif, W., Mauvais, P., Balaguer, P., Rahmani, R., 2006. Activation of alpha- and beta-estrogen receptors by persistent pesticides in reporter cell lines. Life Sci 79, 1160–1169.
[27] Yang, L., Zhou, B., Zha, J., Wang, Z., 2016. Mechanistic study of chlordecone-induced endocrine disruption: based on an adverse outcome pathway network. Chemosphere 161, 372–381.
[28] Mehendale, H.M., 1981. Onset and recovery from chlordecone- and mirex-induced hepatobiliary dysfunction. Toxicol Appl Pharm 58, 132–139.
[29] Cannon, S.B., Kimbrough, R.D., 1979. Short-term chlordecone toxicity in rats including effects on reproduction, pathological organ changes, and their reversibility. Toxicol Appl Pharm 47, 469–476.
[30] Tabet, E., Genet, V., Tiaho, F., Lucas-Clerc, C., Gelu-Simeon, M., Piquet-Pellorce, C., et al., 2016. Chlordecone potentiates hepatic fibrosis in chronic liver injury induced by carbon tetrachloride in mice. Toxicol Lett 255, 1–10.
[31] National Toxicology, P., 1976. Report on carcinogenesis bioassay of technical grade chlordecone (Kepone) (CAS No. 143-50-0). Natl Cancer Inst Carcinog Tech Rep Ser 1976, 1–23.

[32] Sirica, A.E., Wilkerson, C.S., Wu, L.L., Fitzgerald, R., Blanke, R.V., Guzelian, P.S., 1989. Evaluation of chlordecone in a two-stage model of hepatocarcinogenesis: a significant sex difference in the hepatocellular carcinoma incidence. Carcinogenesis 10, 1047–1054.
[33] Fariss, M.W., Blanke, R.V., Saady, J.J., Guzelian, P.S., 1980. Demonstration of major metabolic pathways for chlordecone (kepone) in humans. Drug Metab Dispos 8, 434–438.
[34] Winters, C.J., Molowa, D.T., Guzelian, P.S., 1990. Isolation and characterization of cloned cDNAs encoding human liver chlordecone reductase. Biochemistry 29, 1080–1087.
[35] Belfiore, C.J., Yang, R.S., Chubb, L.S., Lohitnavy, M., Lohitnavy, O.S., Andersen, M. E., 2007. Hepatic sequestration of chlordecone and hexafluoroacetone evaluated by pharmacokinetic modeling. Toxicology 234, 59–72.
[36] Emond, C., Multigner, L., 2022. Chlordecone: development of a physiologically based pharmacokinetic tool to support human health risks assessments. Arch Toxicol 96, 1009–1019.
[37] Delannoy, M., Girardet, J.M., Djelti, F., Yen, F.T., Cakir-Kiefer, C., 2020. Affinity of chlordecone and chlordecol for human serum lipoproteins. Environ Toxicol Pharm 80, 103486.
[38] Soine, P.J., Blanke, R.V., Guzelian, P.S., Schwartz, C.C., 1982. Preferential binding of chlordecone to the protein and high density lipoprotein fractions of plasma from humans and other species. J Toxicol Environ Health 9, 107–118.
[39] Nedellec, V., Rabl, A., Dab, W., 2016. Public health and chronic low chlordecone exposure in Guadeloupe, Part 1: hazards, exposure-response functions, and exposures. Environ Health 15, 75.
[40] Leger, T., Balaguer, P., Le Hegarat, L., Fessard, V., 2023. Fate and PPARgamma and STATs-driven effects of the mitochondrial complex I inhibitor tebufenpyrad in liver cells revealed with multi-omics. J Hazard Mater 442, 130083.
[41] Aninat, C., Piton, A., Glaise, D., Le Charpentier, T., Langouet, S., Morel, F., et al., 2006. Expression of cytochromes P450, conjugating enzymes and nuclear receptors in human hepatoma HepaRG cells. Drug Metab Dispos 34, 75–83.
[42] Gicquel, T., Robert, S., Loyer, P., Victoni, T., Bodin, A., Ribault, C., et al., 2015. IL-1beta production is dependent on the activation of purinergic receptors and NLRP3 pathway in human macrophages. FASEB J 29, 4162–4173.
[43] Xu, L., Hui, A.Y., Albanis, E., Arthur, M.J., O'Byrne, S.M., Blaner, W.S., et al., 2005. Human hepatic stellate cell lines, LX-1 and LX-2: new tools for analysis of hepatic fibrosis. Gut 54, 142–151.
[44] Bronsard, J., Savary, C., Massart, J., Viel, R., Moutaux, L., Catheline, D., et al., 2023. 3D multi-cell-type liver organoids: a new model of non-alcoholic fatty liver disease for drug safety assessments. Toxicol Vitr 94, 105728.
[45] Schymanski, E.L., Jeon, J., Gulde, R., Fenner, K., Ruff, M., Singer, H.P., et al., 2014. Identifying small molecules via high resolution mass spectrometry: communicating confidence. Environ Sci Technol 48, 2097–2098.
[46] Achcar, F., Camadro, J.M., Mestivier, D., 2009. AutoClass@IJM: a powerful tool for Bayesian classification of heterogeneous data in biology. Nucleic Acids Res 37, W63–W67.
[47] Bindea, G., Mlecnik, B., Hackl, H., Charoentong, P., Tosolini, M., Kirilovsky, A., et al., 2009. ClueGO: a cytoscape plug-in to decipher functionally grouped gene ontology and pathway annotation networks. Bioinformatics 25, 1091–1093.
[48] Martin, D., Lobo, F., Lavison-Bompard, G., Guerin, T., Parinet, J., 2020. Effect of home cooking processes on chlordecone content in beef and investigation of its by-products and metabolites by HPLC-HRMS/MS. Environ Int 144, 106077.
[49] Macedo, J.N., Valadares, N.F., Marques, I.A., Ferreira, F.M., Damalio, J.C., Pereira, H.M., et al., 2013. The structure and properties of septin 3: a possible missing link in septin filament formation. Biochem J 450, 95–105.
[50] Zent, E., Vetter, I., Wittinghofer, A., 2011. Structural and biochemical properties of Sept7, a unique septin required for filament formation. Biol Chem 392, 791–797.
[51] Tudor, D., Yu, H., Maupetit, J., Drillet, A.S., Bouceba, T., Schwartz-Cornil, I., et al., 2012. Isotype modulates epitope specificity, affinity, and antiviral activities of anti-HIV-1 human broadly neutralizing 2F5 antibody. Proc Natl Acad Sci USA 109, 12680–12685.
[52] Kim, H.J., Joo, H.J., Kim, Y.H., Ahn, S., Chang, J., Hwang, K.B., et al., 2011. Systemic analysis of heat shock response induced by heat shock and a proteasome inhibitor MG132. PLoS One 6, e20252.
[53] Gerets, H.H., Tilmant, K., Gerin, B., Chanteux, H., Depelchin, B.O., Dhalluin, S., et al., 2012. Characterization of primary human hepatocytes, HepG2 cells, and HepaRG cells at the mRNA level and CYP activity in response to inducers and their predictivity for the detection of human hepatotoxins. Cell Biol Toxicol 28, 69–87.
[54] Starcevic, S.L., Bortolin, S., Woodcroft, K.J., Novak, R.F., 2001. Kepone (chlordecone) disrupts adherens junctions in human breast epithelial cells cultured on matrigel. Vivo 15, 289–294.
[55] Mostowy, S., Cossart, P., 2012. Septins: the fourth component of the cytoskeleton. Nat Rev Mol Cell Biol 13, 183–194.
[56] Ivanov, A.I., Le, H.T., Naydenov, N.G., Rieder, F., 2021. Novel functions of the septin cytoskeleton: shaping up tissue inflammation and fibrosis. Am J Pathol 191, 40–51.
[57] Dolat, L., Hu, Q., Spiliotis, E.T., 2014. Septin functions in organ system physiology and pathology. Biol Chem 395, 123–141.
[58] Hall, P.A., Russell, S.E., 2004. The pathobiology of the septin gene family. J Pathol 204, 489–505.
[59] Spiliotis, E.T., 2018. Spatial effects - site-specific regulation of actin and microtubule organization by septin GTPases. J Cell Sci 131.
[60] Chen, T.Y., Lin, T.C., Kuo, P.L., Chen, Z.R., Cheng, H.L., Chao, Y.Y., et al., 2021. Septin 7 is a centrosomal protein that ensures S phase entry and microtubule nucleation by maintaining the abundance of p150(glued). J Cell Physiol 236, 2706–2724.
[61] Menon, M.B., Sawada, A., Chaturvedi, A., Mishra, P., Schuster-Gossler, K., Galla, M., et al., 2014. Genetic deletion of SEPT7 reveals a cell type-specific role of septins in microtubule destabilization for the completion of cytokinesis. PLoS Genet 10, e1004558.
[62] Fan, Y., Du, Z., Steib, C.J., Ding, Q., Lu, P., Tian, D., et al., 2019. Effect of SEPT6 on the biological behavior of hepatic stellate cells and liver fibrosis in rats and its mechanism. Lab Invest 99, 17–36.
[63] Angelis, D., Spiliotis, E.T., 2016. Septin mutations in human cancers. Front Cell Dev Biol 4, 122.
[64] Liu, M., Shen, S., Chen, F., Yu, W., Yu, L., 2010. Linking the septin expression with carcinogenesis. Mol Biol Rep 37, 3601–3608.
[65] Xu, D., Liu, A., Wang, X., Chen, Y., Shen, Y., Tan, Z., et al., 2018. Repression of Septin9 and Septin2 suppresses tumor growth of human glioblastoma cells. Cell Death Dis 9, 514.
[66] Iwaisako, K., Hatano, E., Taura, K., Nakajima, A., Tada, M., Seo, S., et al., 2008. Loss of Sept4 exacerbates liver fibrosis through the dysregulation of hepatic stellate cells. J Hepatol 49, 768–778.
[67] Wu, Y., Bu, F., Yu, H., Li, W., Huang, C., Meng, X., et al., 2017. Methylation of Septin9 mediated by DNMT3a enhances hepatic stellate cells activation and liver fibrogenesis. Toxicol Appl Pharm 315, 35–49.
[68] Hu, Q., Nelson, W.J., Spiliotis, E.T., 2008. Forchlorfenuron alters mammalian septin assembly, organization, and dynamics. J Biol Chem 283, 29563–29571.
[69] Angelis, D., Karasmanis, E.P., Bai, X., Spiliotis, E.T., 2014. In silico docking of forchlorfenuron (FCF) to septins suggests that FCF interferes with GTP binding. PLoS One 9, e96390.
[70] Shi, X., Li, J., Zou, X., Greggain, J., Rodkaer, S.V., Faergeman, N.J., et al., 2013. Regulation of lipid droplet size and phospholipid composition by stearoyl-CoA desaturase. J Lipid Res 54, 2504–2514.
[71] Carpenter, H.M., Hedstrom, O.R., Siddens, L.K., Duimstra, J.R., Cai, Z.W., Fisher, K. A., et al., 1996. Ultrastructural, protein, and lipid changes in liver associated with chlordecone treatment of mice. Fundam Appl Toxicol 34, 157–164.
[72] Kesisova, I.A., Robinson, B.P., Spiliotis, E.T., 2021. A septin GTPase scaffold of dynein-dynactin motors triggers retrograde lysosome transport. J Cell Biol 220.
[73] Song, P.X., Peng, J., Omrane, M., Cai, T.T., Samuel, D., Gassama-Diagne, A., 2022. Septin 9 and phosphoinositides regulate lysosome localization and their association with lipid droplets. iScience 25, 104288.
[74] Akil, A., Peng, J., Omrane, M., Gondeau, C., Desterke, C., Marin, M., et al., 2016. Septin 9 induces lipid droplets growth by a phosphatidylinositol-5-phosphate and microtubule-dependent mechanism hijacked by HCV. Nat Commun 7, 12203.
[75] Scorletti, E., Carr, R.M., 2022. A new perspective on NAFLD: focusing on lipid droplets. J Hepatol 76, 934–945.
[76] Fromenty, B., 2019. Inhibition of mitochondrial fatty acid oxidation in drug-induced hepatic steatosis. Liver Res 3, 157–169.
[77] Gluchowski, N.L., Becuwe, M., Walther, T.C., Farese, R.V., Jr, 2017. Lipid droplets and liver disease: from basic biology to clinical implications. Nat Rev Gastroenterol Hepatol 14, 343–355.
[78] Aubert, J., Begriche, K., Knockaert, L., Robin, M.A., Fromenty, B., 2011. Increased expression of cytochrome P450 2E1 in nonalcoholic fatty liver disease: mechanisms and pathophysiological role. Clin Res Hepatol Gastroenterol 35, 630–637.
[79] Fitian, A.I., Nelson, D.R., Liu, C., Xu, Y., Ararat, M., Cabrera, R., 2014. Integrated metabolomic profiling of hepatocellular carcinoma in hepatitis C cirrhosis through GC/MS and UPLC/MS-MS. Liver Int 34, 1428–1444.
[80] Wanders, R.J., Komen, J., Kemp, S., 2011. Fatty acid omega-oxidation as a rescue pathway for fatty acid oxidation disorders in humans. FEBS J 278, 182–194.
[81] Fromenty, B., Roden, M., 2023. Mitochondrial alterations in fatty liver diseases. J Hepatol 78, 415–429.
[82] Reddy, J.K., Rao, M.S., 2006. Lipid metabolism and liver inflammation. II. Fatty liver disease and fatty acid oxidation. Am J Physiol Gastrointest Liver Physiol 290, G852–G858.
[83] Moore, M.P., Cunningham, R.P., Meers, G.M., Johnson, S.A., Wheeler, A.A., Ganga, R.R., et al., 2022. Compromised hepatic mitochondrial fatty acid oxidation and reduced markers of mitochondrial turnover in human NAFLD. Hepatology 76, 1452–1465.
[84] Rao, M.S., Reddy, J.K., 2001. Peroxisomal beta-oxidation and steatohepatitis. Semin Liver Dis 21, 43–55.
[85] Talari, N.K., Mattam, U., Meher, N.K., Paripati, A.K., Mahadev, K., Krishnamoorthy, T., et al., 2023. Lipid-droplet associated mitochondria promote fatty-acid oxidation through a distinct bioenergetic pattern in male Wistar rats. Nat Commun 14, 766.
[86] Li, Z.Z., Berk, M., McIntyre, T.M., Feldstein, A.E., 2009. Hepatic lipid partitioning and liver damage in nonalcoholic fatty liver disease: role of stearoyl-CoA desaturase. J Biol Chem 284, 5637–5644.
[87] Anthierieu, S., Rogue, A., Fromenty, B., Guillouzo, A., Robin, M.A., 2011. Induction of vesicular steatosis by amiodarone and tetracycline is associated with up-regulation of lipogenic genes in HepaRG cells. Hepatology 53, 1895–1905.
[88] Teo, S., Vore, M., 1991. Mirex inhibits bile acid secretory function in vivo and in the isolated perfused rat liver. Toxicol Appl Pharm 109, 161–170.
[89] Gottlieb, A., Canbay, A., 2019. Why bile acids are so important in non-alcoholic fatty liver disease (NAFLD) progression. Cells 8.
[90] Tanaka, N., Matsubara, T., Krausz, K.W., Patterson, A.D., Gonzalez, F.J., 2012. Disruption of phospholipid and bile acid homeostasis in mice with nonalcoholic steatohepatitis. Hepatology 56, 118–129.
[91] Lake, A.D., Novak, P., Shipkova, P., Aranibar, N., Robertson, D., Reily, M.D., et al., 2013. Decreased hepatotoxic bile acid composition and altered synthesis in progressive human nonalcoholic fatty liver disease. Toxicol Appl Pharm 268, 132–140.

[92] Puri, P., Daita, K., Joyce, A., Mirshahi, F., Santhekadur, P.K., Cazanave, S., et al., 2018. The presence and severity of nonalcoholic steatohepatitis is associated with specific changes in circulating bile acids. Hepatology 67, 534–548.
[93] Kalhan, S.C., Guo, L., Edmison, J., Dasarathy, S., McCullough, A.J., Hanson, R.W., et al., 2011. Plasma metabolomic profile in nonalcoholic fatty liver disease. Metabolism 60, 404–413.
[94] Kakehashi, A., Stefanov, V.E., Ishii, N., Okuno, T., Fujii, H., Kawai, K., et al., 2017. Proteome characteristics of non-alcoholic steatohepatitis liver tissue and associated hepatocellular carcinomas. Int J Mol Sci 18.
[95] Jamwal, R., de la Monte, S.M., Ogasawara, K., Adusumalli, S., Barlock, B.B., Akhlaghi, F., 2018. Nonalcoholic fatty liver disease and diabetes are associated with decreased CYP3A4 protein expression and activity in human liver. Mol Pharm 15, 2621–2632.
[96] Rizner, T.L., Penning, T.M., 2014. Role of aldo-keto reductase family 1 (AKR1) enzymes in human steroid metabolism. Steroids 79, 49–63.
[97] Gelu-Simeon, M., Lafrance, M.J., Michineau, L., Saillard, E., Thome, J.P., Emond, C., et al., 2024. Inverse association between plasma chlordecone concentrations and progression of alcoholic liver fibrosis: the role of liver metabolism. Environ Health 23, 30.
[98] Resiere, D., Lapostolle, F., Florentin, J., Banydeen, R., Gueye, P., Pujo, J., et al., 2024. A health strategy for chlordecone (Kepone) exposure in the French Territories of America. Lancet.